Int J Earth Sci (Geol Rundsch) (2016) 105:1707–1728
DOI 10.1007/s00531-015-1146-6

ORIGINAL PAPER

Long-term cooling history of the Albertine Rift: new evidence from the western rift shoulder, D.R. Congo

F. U. Bauer · U. A. Glasmacher · U. Ring · R. W. Grobe · V. S. Mambo · M. Starz

Received: 27 November 2013 / Accepted: 17 January 2015 / Published online: 1 February 2015

Abstract To determine the long-term landscape evolution of the Albertine Rift in East Africa, low-temperature thermochronology was applied and the cooling history constrained using thermal history modelling. Acquired results reveal (1) "old" cooling ages, with predominantly Devonian to Carboniferous apatite fission-track ages, Ordovician to Silurian zircon (U–Th)/He ages and Jurassic to Cretaceous apatite (U–Th–Sm)/He ages; (2) protracted cooling histories of the western rift shoulder with major phases of exhumation in mid-Palaeozoic and Palaeogene to Neogene times; (3) low Palaeozoic and Neogene erosion rates. This indicates a long residence time of the analysed samples in the uppermost crust, with the current landscape surface at a near-surface position for hundreds of million years. Apatite He cooling ages and thermal history models indicate moderate reheating in Jurassic to Cretaceous times. Together with the cooling age distribution, a possible Albertine high with a distinct relief can be inferred that might have been a source area for the Congo Basin.

Keywords East African Rift System · Albertine Rift · Low-temperature thermochronology · Apatite fission-track · Thermal history modelling · Long-term landscape evolution

Electronic supplementary material The online version of this article (doi:10.1007/s00531-015-1146-6) contains supplementary material, which is available to authorized users.

F. U. Bauer (✉) · U. A. Glasmacher · M. Starz
Institute of Earth Sciences, Heidelberg University, 69120 Heidelberg, Germany
e-mail: Friederike.Bauer@geo.uib.no

U. A. Glasmacher
e-mail: Ulrich.A.Glasmacher@geow.uni-heidelberg.de

Present Address:
F. U. Bauer
Department of Earth Science, University of Bergen, 5007 Bergen, Norway

U. Ring
Department of Geological Sciences, Stockholm University, 106 91 Stockholm, Sweden

R. W. Grobe
GeoThermal Engineering GmbH, 76133 Karlsruhe, Germany

V. S. Mambo
Faculty of Science, Ruwenzori State University, B.P. 560, Butembo, D.R. Congo

Introduction

Surface uplift, deep weathering and erosion are amongst the dominant surface processes that have shaped the African continent over the past 450 Ma (Petters 1991). As a former part of the supercontinent Gondwana, the African continent preserves evidence of a long geological record, including plate reconfigurations with accretion of old cratonic masses, as well as different phases of rifting and glaciation (e.g. Burgoyne et al. 2005; Burke et al. 2003; Catuneanu et al. 2005). In East Africa, the Cenozoic East African Rift System (EARS) forms a striking geomorphologic and tectonic feature that is still active today (Fig. 1). It provides a suitable natural laboratory to study rift processes and associated landscape changes through time.

Rifting in general is accompanied by (localized) rock uplift along the rift shoulders and associated erosion (cf. Royden and Keen 1980; Rowley and Sahagian 1986; Kusznir and Ziegler 1992; Karner et al. 2000; Sachau and Koehn 2010). The upward-directed movement results in the creation of highly elevated landscapes, with the generated

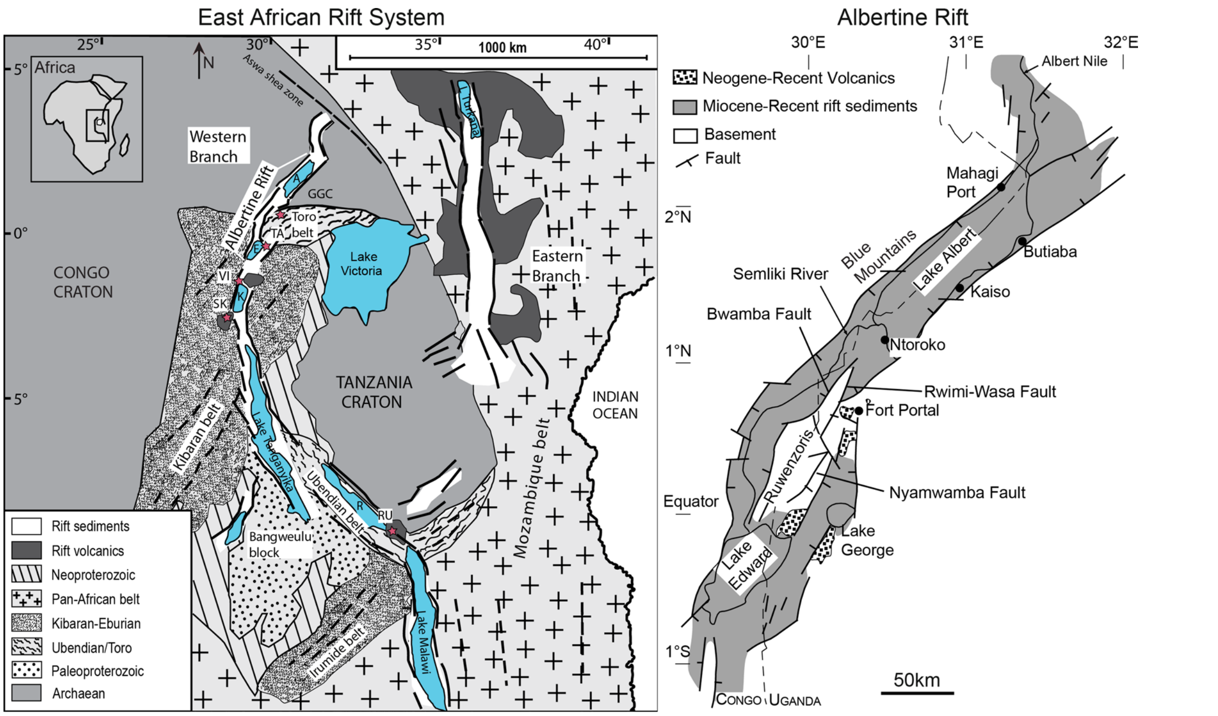

Fig. 1 *Left* simplified structural map of the EARS with location of the Albertine Rift and Rwenzori Mtns (modified after Aanyu 2011). Sites of specific volcanic provinces (*asterisks*), rift basins and lakes are outlined; *A* Lake Albert, *E* Lake Edward, *K* Lake Kivu, *R* Lake Rukwa; *TA* Toro-Ankole, *VI* Virunga, *SK* south Kivu, *RU* Rungwe volcanic provinces. *Right* simplified geological map of the Albertine Rift with main localities (modified after Ring 2008)

topography prone to erosion followed by isostatic rebound (Kusznir and Ziegler 1992). Such a coupling of deep-seated and surface processes dynamically shapes the Earth's surface and exerts a strong control on long-term landscape evolution.

To understand the morphological evolution of a region, knowledge about phases of (dis-) equilibrium between rock exhumation and rock uplift governed by surface (e.g. climatic) and deep-seated (e.g. tectonic) processes is essential. Low-temperature thermochronology (LTT) provides well-established techniques to trace rock displacements through the upper crust and to study the long-term morphological evolution of a landscape (e.g. Reiners and Shuster 2009).

In previous LTT studies, the thermal (exhumation) history of the Albertine Rift was traced back to the Palaeozoic. Evidence for Silurian to Devonian cooling was recorded in the Rwenzori Mtns that are located in the Albertine Rift (MacPhee 2006; Bauer et al. 2010b, 2013). The Rwenzori Mtns, a metamorphic basement block of more than 5 km height, reveal a much older thermal history than expected for a high-altitude Neogene extensional setting. The new data from eastern Congo follow this trend, disclosing a protracted thermal history and calling into question whether there was significant post-Palaeozoic erosion along the rift shoulder.

Here, we present the first LTT data from the western rift shoulder of the Albertine Rift in the eastern Democratic Republic of the Congo (DRC), including apatite fission-track data (AFT), apatite and zircon (U–Th–Sm)/He data (AHe, ZHe) and thermal history models. We discuss their significance for the exhumation history of the Albertine Rift and the long-term landscape evolution of the area.

Regional geological setting and landscape

Basement geology

Africa's geological record spans more than 3.8 Ga and includes several orogenic cycles (Petters 1991). The major Precambrian tectono-metamorphic cycles and resulting high-grade metamorphic belts in Africa are the Pan-African (~700–500 Ma), Kibaran (~1,200–900 Ma), Ubendian (~2.0–1.8 Ga) and Archean (>2.5 Ga) cycles (cp. Appel et al. 2005; Fritz et al. 2005). In East Africa, the Archean Congo and Tanzania cratons acted as rigid blocks while the flanking mobile belts experienced metamorphism and deformation during successive orogeneses (Fig. 1). The resulting lithological and tectonic complexes together with the Archean cratons characterize the basement geology of East Africa, where Archean and Proterozoic basement rocks are widely exposed. In the Albertine Rift, the cratonic crust between the Congo and Tanzania cratons consists of a late Archean (~2.6 Ga) WSW to ENE trending fold and thrust belt with a complex structural framework (Link et al. 2010). Since the end of the Pan-African orogeny, the tectonic evolution of the African continent was dominated by rift processes (Delvaux 1991). Inherited Precambrian and early Palaeozoic basement fabrics have an important control on the later rifting events, like the Permo-Triassic to Jurassic Karoo rifting and the Neogene rifting of the EARS with the Albertine Rift in particular (Delvaux 2001; Macheyeki et al. 2008; Aanyu and Koehn 2011).

Albertine Rift: Western Branch East African Rift System

The East African Rift System (EARS) forms a prominent structure, with an eastern and a western branch, striking approximately N–S and extending from Ethiopia to Mozambique (Fig. 1) (Ebinger et al. 2013; Ring 2014). The western branch (i.e. western rift) extends from Uganda to Malawi and created a series of rift basins with Lake Albert in the northernmost part (e.g. Schlueter 1997). The onset of rifting in the western branch is still debated. Evidence of volcanic activity indicates diachronous rifting that commenced in the mid-Miocene in the central part, with rift propagation both to the north (~12 Ma) and to the south (~7 Ma) (Ebinger 1989; Kampunzu et al. 1998; Morley 1999; Ebinger and Furman 2002). Roberts et al. (2012) propose an earlier onset of rifting (~25 Ma), contemporaneous with the eastern branch. The western branch is characterized by deep rift lakes and steep fault scarps rising up thousands of metres adjacent to the graben floor and shows minor volcanic activity compared to the eastern branch (Upcott et al. 1996; Schlueter 1997; Karner et al. 2000).

The Albertine Rift is the northern part of the western branch and comprises individual basins, such as Lake Albert, Lake Edward, Semliki Valley and Lake George basins (Bahat and Mohr 1987; Karner et al. 2000; Ring 2008) (Fig. 1). Between Lake Albert and Lake Edward, the Rwenzori Mtns raise to more than 5 km asl (above sea level). This Precambrian metamorphic basement block is framed by two rift sub-segments, the southward propagating Lake Albert sub-segment and the northward propagating Lake Edward/George sub-segment (Aanyu and Koehn 2011). Along their north-eastern side, the Rwenzoris are connected to the eastern rift shoulder forming a promontory (Fig. 1).

The Rwenzori Mtns are truncated by N–S, NW–SE, NE–SW and E–W trending normal faults, locally with a significant strike-slip component (McConnell 1959; Ring 2008; Koehn et al. 2010). The various fault systems cut through the Rwenzoris, dissecting them into several blocks. The main lithologies are gneiss, schist and amphibolite. Subordinate intrusive rocks with a variable metamorphic overprint, quartzite and marble of Precambrian age are exposed as well (Michot 1938; Tanner 1971; Bauer et al. 2012). Similar rock types can be found along the western rift shoulder, as the lithological units are roughly striking NE–SW. In the area west of Lake Edward, meta-sediments, gneiss, schist and migmatite of the northern Kibaran belt are exposed. To the north, the rocks of the Mesoproterozoic Kibaran belt are intersected by Palaeoproterozoic terranes, resulting in a complex geology with patches of Palaeo-, Meso- and Neoproterozoic rocks (Fig. 2) (Tack et al. 2010). Along the rift shoulders and on downthrown basement blocks in the rift valley, intense deformation is evident (Fig. 3). In the Blue Mountains west of Lake Albert, mainly granites are exposed. They are often deeply weathered and crosscut by mafic dikes (Fig. 3) (Bauer et al. 2010a). Locally, Phanerozoic sedimentary and volcanic rocks cover the Precambrian basement. Sandstones, shales and siltstones of Permo-Carboniferous age (Lepersonne 1974) are exposed in depressions along the easternmost margin of the Congo Basin (Figs. 2, 3). Along the rift shoulders of the Albertine Rift, Cenozoic volcanic rocks and lateritic soils locally cover the Precambrian igneous and metamorphic basement rocks, while the rift valley is filled with fluvial, lacustrine and volcaniclastic material. Continuous Neogene sedimentary successions crop out along the rift escarpments (Fig. 3), with a maximum exposed thickness of ~200–600 m (Pickford et al. 1993). The oldest sediments in the Lake Albert basin are late Miocene in age (Pickford et al. 1993; Ovington and Burdon 2009; Roller et al. 2010). In depressions of the Rwenzori Mtns, Pleistocene to Holocene glacial sediments were recorded (Livingstone 1967).

Glaciations: After the Precambrian and early Palaeozoic tectonic events ceased, rifting processes, rock and surface uplift, deep weathering and erosion were the dominant processes affecting the African continent over the last 450 Ma (Petters 1991). Africa experienced drastic climate changes that range from the Neoproterozoic Snowball Earth to a hot climate in the Cretaceous. Prominent Palaeozoic glaciations include the Ordovician Sahara glaciation in North Africa (440 Ma) and the Late Palaeozoic Gondwana glaciations (~350–250 Ma) (Eyles 2008). The distribution of the Permo-Carboniferous glaciers is not entirely resolved, assuming either a large ice sheet covering southern Gondwana or patchy distributed ice sheets across Gondwana (Isbell et al. 2012). Equivalent siliciclastic Karoo deposits were also reported for Uganda and the Congo Basin (Schlueter et al. 1993; Catuneanu et al. 2005; Bradley et al. 2010). By the end of the Palaeozoic, the African continent had moved from a polar to a more equatorial position. Despite the equatorial position, high peak areas of the East African Mountains, e.g. Kilimanjaro and Rwenzori Mtns, were glaciated in Neogene times. Present landforms

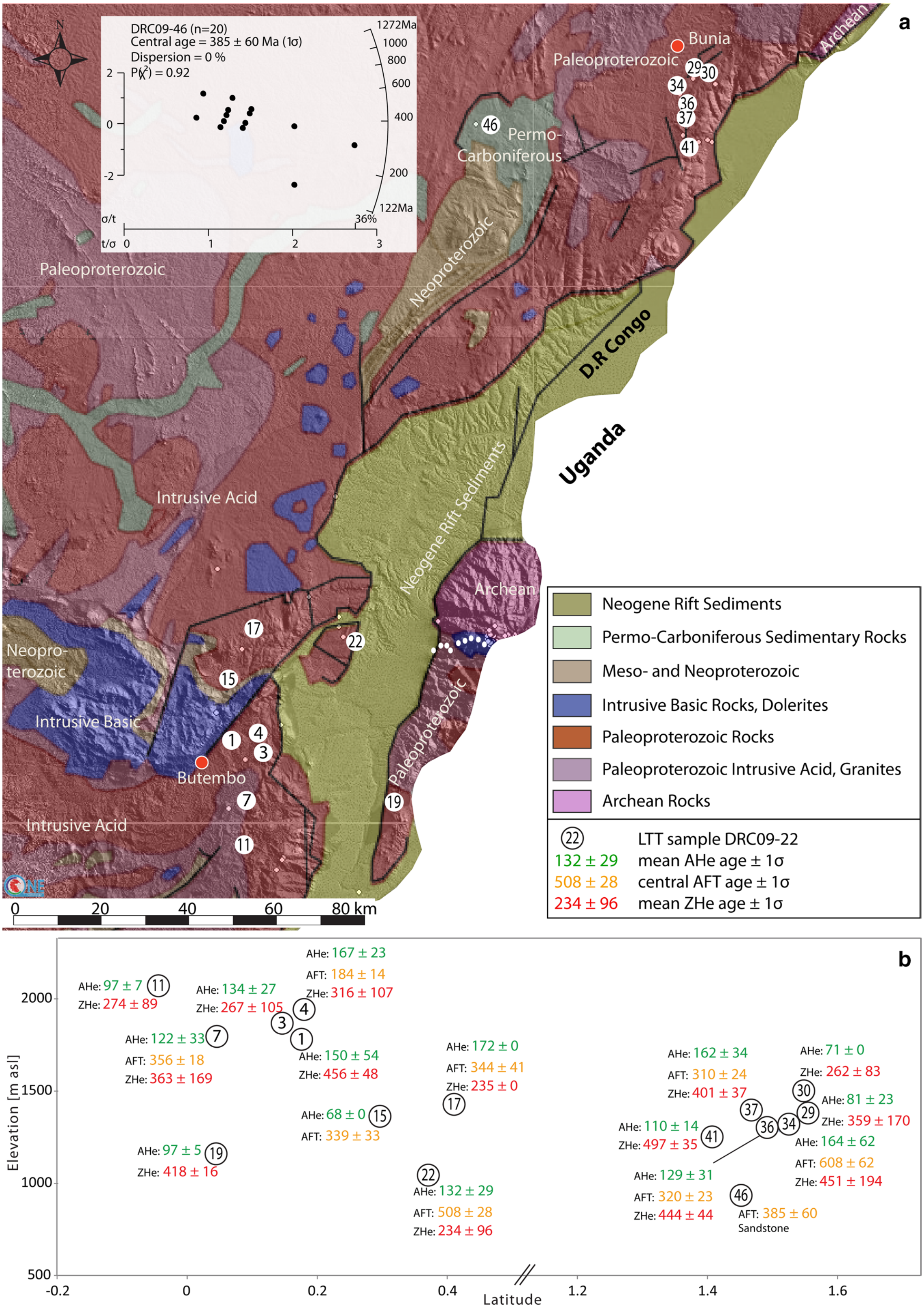

and the relief of the Rwenzori Mtns bear witness of several Pleistocene and Holocene glacial cycles; the high peaks down to about 2,500 m were covered by glaciers, while the surrounding areas of the Albertine Rift show no evidence for Neogene glaciations (Whittow 1966; Ollier and Pain 2000; Osmaston and Harrison 2005).

◀ **Fig. 2** **a** DEM from SRTM data with a geological map from the eastern DRC (geological map based upon 1:2.000.000 Lithostratigraphy and Chronostratigraphy map of the Democratic Republic of Congo, Geological Survey of DRC, with the permission of OneGeology). White dots are sample sites, and numbers show sample locations in eastern DRC up to Blue Mountains at Lake Albert with low-temperature thermochronology (LTT) data displayed in Fig. 2b. Apatite He and zircon He (AHe, ZHe) data are plotted as mean He age ±1σ sample standard deviation of the mean, apatite fission-track (AFT) data plotted as central age ±1σ; radial plot for sandstone sample DRC09-46 shows the single-grain age distribution (radial plotter, Vermeesch 2009). **b** Samples and LTT ages plotted along the rift shoulder with their specific height. Latitude from south to north not to scale between 0.4° and 1.2°, elevation exaggerated; legend in Fig. 2a for details on cooling age display

Previous thermochronology studies: thermal evolution Rwenzori Mtns

Thermochronology studies in the Albertine Rift were previously conducted by MacPhee (2006) ((U–Th)/He and U–Pb thermochronometry) and Bauer et al. (2010b, 2013) (fission-track and (U–Th–Sm)/He thermochronometry together with thermal history modelling) (Fig. 4).

On the basis of morphological evidence, cooling age distribution and thermal history modelling, different areas are distinguished along the Rwenzori Mtns. From north to south, a northern, a central and a southern part can be

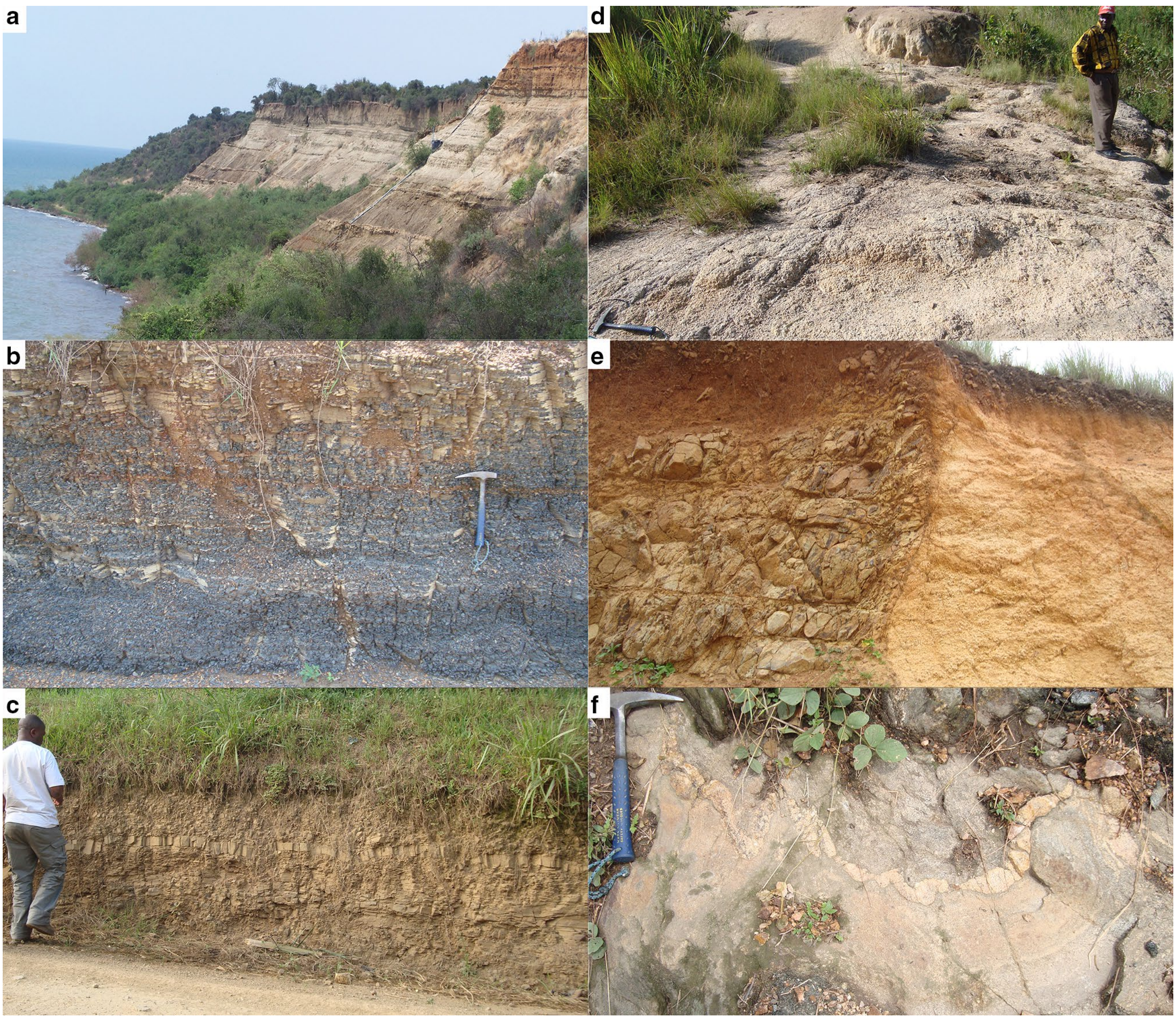

Fig. 3 Selected rock types observed on the western rift shoulder and shore of Lake Albert. **a** Neogene sediments from the eastern shore of Lake Albert, similar to the sediments from the western shore (620 m asl); **b** shale with siltstones exposed in a depression along the easternmost margin of the Congo Basin (895 m asl, close to **c**); **c** thinly banked sandstones (935 m asl, DRC09-46), **b**, **c** Permo-Carboniferous in age (after Lepersonne 1974), **d** deeply weathered granites, Blue Mountains, close to DRC09-34 (1,505 m asl); **e** basic dike cutting through granites, Blue Mountains, close to DRC09-36 (1,453 m asl); **f** granitic gneiss with intense deformation, down-faulted block, Semliki rift valley, close to DRC09-22 (1,049 m asl)

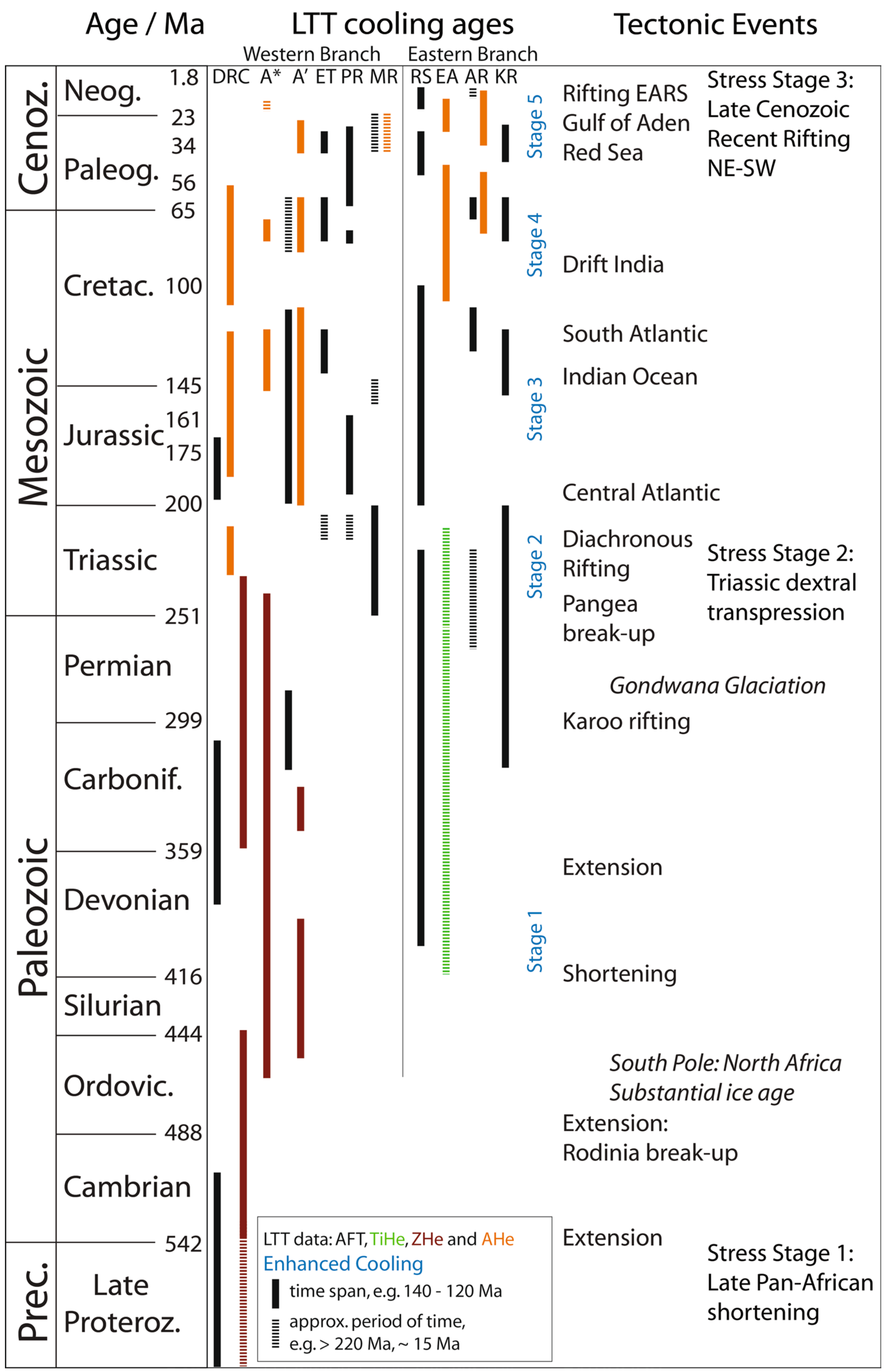

Fig. 4 Compilation of low-temperature thermochronology (LTT) cooling ages from the EARS (western and eastern branch) together with tectonic events, glaciations (Fabre 1988; Badalini et al. 2002; Bumby and Guiraud 2005) and stress stages (Delvaux 1991; Delvaux et al. 2012) affecting the East African geological evolution (modified after Bauer et al. 2013). LTT data are shown as age ranges with modelled periods of enhanced cooling (*blue*); apatite fission-track (AFT, *black*); (U–Th–Sm)/He data of titanite (TiHe, *green*); zircon (ZHe, *red*), apatite (AHe, *yellow*). LTT study locations: DRC: western rift shoulder, Albertine Rift; *A** Albertine Rift (by MacPhee), *A′* Albertine Rift (by Bauer et al.), *ET* east Tanzania, *PR* Pangani Rift, *MR* Malawi Rift, *RS* Red Sea Rift, *EA* Afar, *AR* Anza Rift, *KR* Kenya Rift (Wagner et al. 1992; Foster and Gleadow 1992, 1996; Noble et al. 1997; van der Beek et al. 1998; Mbede 2001; Abbate et al. 2002; Pik et al. 2003, 2008; Spiegel et al. 2004, 2007; MacPhee 2006; Bauer et al. 2010b, 2013 and this study)

distinguished. The central Rwenzoris are further subdivided into a northern and a southern block (Bauer et al. 2013). The subdivision of the central Rwenzoris into different blocks is mainly based on fission-track and (U–Th–Sm)/He cooling ages and derived cooling histories. The two blocks in the central Rwenzoris are separated by a presumedly NW–SE trending fault set. The northern block yielded distinctly younger apatite fission-track ages (~130 Ma) than the southern block (~300 Ma). Cooling ages in both blocks do not vary significantly with elevation, despite a relief of more than 3 km. From thermal history modelling, a protracted cooling history was derived. Time–temperature cooling histories point to i) the existence of decoupled blocks, ii) the reactivation of pre-existing structures inherited from Palaeozoic folding and thrusting and iii) the relocation of individual blocks along distinct fault planes. The LTT data suggest that the Rwenzoris experienced a prolonged and complex cooling (i.e. exhumation) history that can be traced back to Palaeozoic times (Bauer et al. 2013), with the last major tectono-thermal perturbation in the Palaeoproterozoic (U–Pb, ~1.9 Ga; MacPhee 2006). Several periods of exhumation/cooling were determined for the Rwenzoris that match local or regional tectonic events (Fig. 4) (MacPhee 2006; Bauer et al. 2010b, 2013). Inherited basement fabrics have most likely influenced the structural and thermal evolution of the Rwenzoris.

The different periods of cooling that affected the Rwenzoris comprise an initial phase in the Palaeozoic (Silurian to Devonian) followed by Mesozoic and Cenozoic cooling events. The Rwenzoris were not exhumed as a coherent block (Bauer et al. 2013). The pre-Neogene evolution was triggered by tectonic processes like the opening of the Indian Ocean and the South Atlantic (Fig. 4). Several lines of evidence point to the presence of faults and fault-related movements in the Rwenzoris, for example the dissected morphology and the different generations of fault sets (Ring 2008). Fault-related movements of Permo-Carboniferous (~300 Ma), early Jurassic (~190 Ma) and late Cretaceous (~90 Ma) age were revealed by offsets in AFT ages. Bauer et al. (2013) suggested the possibility of a Mesozoic topographic Albertine high. In the Cenozoic, the EARS was established, resulting in differential surface uplift in the Albertine Rift, with pronounced movements along the western flank of the Rwenzori Mtns (MacPhee 2006; Ring 2008; Bauer et al. 2010b, 2013). Detrital thermochronology data (Bauer et al. 2013) support a late Neogene exhumation, in accordance with increased Neogene sedimentation rates (Roller et al. 2012) and palaeontological constraints (Pickford et al. 1993). The exhumation of the Rwenzoris most likely was accompanied by surface uplift, allowing for glaciations (Ring 2008; Kaufmann and Romanov 2012). The final rock and surface uplift that shaped the Rwenzoris are attributed to a fast process, associated with erosion along predefined fault zones (Bauer et al. 2013).

Methods

During a field-campaign in 2009, we collected a set of 46 samples from the western rift shoulder of the Albertine Rift (eastern DRC). We sampled along one N–S and several E–W trending transects, covering the area from northern Lake Edward up to Lake Albert (N–S), with transects branching off to the east, across the escarpment and into the rift valley towards the Rwenzori Mtns (Fig. 2). Elevations range from 780 to 2,600 m asl. The sampling was often hampered by dense vegetation and deep weathering. The latter was frequently observed in the area of Bunia and Lake Albert in the north (Bauer et al. 2010a). Processed lithologies mainly comprise Precambrian granites, migmatites, gneisses and schists, as well as some late Palaeozoic sandstones from the margin of the Congo Basin (Figs. 2, 3).

We obtained cooling ages from 9 apatite fission-track (AFT) samples, 15 apatite (U–Th–Sm)/He (AHe) samples and 14 zircon (U–Th)/He (ZHe) samples. Whenever possible we analysed the same sample for multiple thermochronometers. The results are reported in Tables 1, 2 and 3. For sample preparation, we followed the general heavy mineral separation routine as, e.g. described by Donelick et al. (2005). AFT analyses were performed at Heidelberg and He analyses at the Arizona Radiogenic Helium Dating Laboratory (ARHDL; University of Arizona). For details of the analytical procedures, we refer to Reiners and Nicolescu (2006) and Bauer et al. (2013) and literature cited therein. More detailed summaries on LTT techniques are provided by Reiners and Brandon (2006), Lisker et al. (2009) and Green et al. (2013).

Apatite fission-track thermochronology

Apatite fission-track (AFT) thermochronology is based on spontaneous fission of naturally occurring ^{238}U, leaving chemically etchable latent tracks in minerals and natural glasses (Wagner 1972). To reveal the thermal history of a sample by AFT dating, the track density (etch pit areal density at an artificially polished internal surface) and the track length distribution of horizontal confined tracks (CT) are used (e.g. Wagner and Van den haute 1992; Lisker et al. 2009). Fission-tracks in apatite anneal depending on time–temperature conditions, the AFT closure temperature is ~110 °C (for cooling rates of 1 °C/Ma and a holding time of ~10 Ma) (Green and Durrani 1977; Green 1981, 1988; Laslett et al. 1984; Donelick et al. 1999). Depending on the apatite's chemical composition, the partial annealing zone (PAZ) ranges from ~120 to 60 °C (e.g. Gleadow and Duddy 1981; Reiners et al. 2005). The fission-track annealing kinetics of apatite are influenced by the fluorine and chlorine content (e.g. Green et al. 1986). Apart from direct measurements of the Cl content (electron microprobe analysis), the etch pit diameter (D_{par}) can be used as an alternative parameter to estimate the annealing kinetics. Cl-rich apatites generally are more resistant to annealing and show larger etch pits than fluorapatite (Donelick et al. 2005).

Apatite and zircon (U–Th–Sm)/He thermochronology

Apatite and zircon (U–Th–Sm)/He thermochronology (He dating) is based on the concentration of accumulated ^{4}He

Table 1 Summary of apatite fission-track data and sample locations with description, western Albertine Rift

Sample	Elev. (m asl)	Latitude	Longitude	Lithology	U (µg/g)	std (µg/g)	*n*	Sp. Tracks		Ind. Tracks		$P(\chi^2)$ (%)	Central age (Ma)	1σ (Ma)
								ρs	Ns	ρi	Ni			
Southern area/West of Rwenzori														
DRC09-01	1,775	0.17606	29.34545	gn	–	–	–	–	–	–	–	–	–	–
DRC09-03	1,863.1	0.15003	29.40984	gn	–	–	–	–	–	–	–	–	–	–
DRC09-04$^{\#}$	1,944.1	0.18043	29.40423	gn	16.0	5.3	22	14.659	4902	14.979	5009	0.0	184.2	14.3
DRC09-07*	1,807.2	0.04633	29.37877	sh-gn	8.9	1.9	24	16.354	4366	7.593	2027	6.5	355.6	18.0
DRC09-11	2,068.6	−0.04271	29.38687	migm	–	–	–	–	–	–	–	–	–	–
DRC09-15*	1,365.7	0.29820	29.34112	gr-gn	2.1	0.9	30	3.706	369	1.858	185	98.8	338.5	33.2
DRC09-17$^{\#}$	1,426.0	0.40484	29.39330	au-gn	1.6	1.1	22	2.588	527	1.596	325	0.03	343.6	41.0
DRC09-19	1,157.5	0.04720	29.68323	gn	–	–	–	–	–	–	–	–	–	–
DRC09-22$^{\#}$	1,049.6	0.37152	29.61497	gn gr-gn	5.5	1.4	23	15.160	2946	5.861	1139	8.2	507.8	28.1
Northern area/West of Lake Albert														
DRC09-29	1,411.1	1.55439	30.31677	gr	–	–	–	–	–	–	–	–	–	–
DRC09-30	1,505.3	1.54643	30.32661	gr	–	–	–	–	–	–	–	–	–	–
DRC09-34$^{\#}$	1,310.4	1.51613	30.27173	gr	5.0	1.9	23	16.543	2219	5.621	754	0.0	607.5	62.1
DRC09-36$^{\#}$	1,301.7	1.49512	30.28084	gr	3.8	1.3	19	6.033	963	3.828	611	5.6	319.8	23.2
DRC09-37$^{\#}$	1,395.7	1.46683	30.28681	gr	29.5	25.4	18	42.197	2283	30.978	1676	0.0	309.5	23.6
DRC09-41	1,254.9	1.40777	30.29754	gr-bt-gn	–	–	–	–	–	–	–	–	–	–
DRC09-46*	935.5	1.44658	29.88286	sst	2.1	2.3	20	4.078	142	1.809	63	91.7	384.8	60.2

Sample location, elevation in metre above sea level, latitude and longitude (WGS 84); Lith., lithology; au-gn, augen-gneiss; bt-gn, biotite gneiss; gn, gneiss; gr, granite; gr-gn, granitic gneiss; migm, migmatite; sh, schist; sst, sandstone; –, not analysed by apatite fission-track; U, std: uranium concentration and standard deviation in µg/g; *n,* number of counted apatite grains; ρs, density of spontaneous tracks (10^5 tr/cm^2); Ns, number of spontaneous tracks; ρi, density of induced tracks (10^5 tr/cm^2); Ni, number of induced tracks; $P(\chi^2)$, probability that single-grain ages are consistent and belong to the same population. Test is passed if $P(\chi^2) > 5$ % (Galbraith 1981). Ages were calculated with TrackKey 4.2 (Dunkl 2002) using a ζ value of 339.57 ± 12.85 (Starz); tracks counted on CN5 dosimeter glass (Nd) are marked by superscripts. Nd^{*} = 15,216 tracks, $Nd^{\#}$ = 15,654 tracks

AFT grain mounts were etched in 5.5 N HNO_3 for 20 ± 1 s at 20 ± 1 °C and afterwards covered by U-free detection muscovite. The sample batch plus two Durango apatite age standards and three glass neutron dosimeter (CN5, top, middle and bottom of sample batch) were irradiated at the research reactor FRM II, Munich. After irradiation, the detection mica were etched in 48 % HF for 20 ± 0.1 min at 20 ± 1 °C

Table 2 Apatite fission-track length data, western Albertine Rift

Sample	n CT	CT mean (µm)	CT std (µm)	CT skew	L_c mean (µm)	L_c std (µm)	L_c skew	n D_{par} (µm)	D_{par} Mean (µm)	D_{par} std	D_{par} skew
DRC-09-04	99	10.8	1.9	0.03	12.5	1.5	−0.42	172	1.2	0.2	0.07
DRC-09-07	116	10.6	1.9	0.2	12.7	1.3	−0.10	92	1.2	0.2	0.35
DRC-09-15	3	8.2	1.5	−0.20	11.3	0.8	−1.34	129	1.4	0.5	1.49
DRC-09-17	2	8.0	0.6	n.d.	11.4	0.3	n.d.	80	1.1	0.3	1.97
DRC-09-22	12	9.5	2.0	0.80	11.7	1.9	−1.04	88	1.3	0.3	1.10
DRC-09-34	14	11.3	2.4	0.56	12.7	2.0	0.26	100	1.6	0.3	0.88
DRC-09-36	6	9.1	1.4	0.29	11.6	1.5	−0.27	101	1.3	0.2	0.43
DRC-09-37	60	10.3	2.0	0.63	11.7	1.8	−0.53	199	1.2	0.3	3.89
DRC-09-46	n.d.	n.d.	n.d.	n.d.	n.d.	n.d.	n.d.	2	1.4	n.d.	n.d.

n CT, number of confined tracks measured; CT mean, mean confined track length, std: standard deviation; skew., skewness of distribution relative to the mean value (measure of asymmetry of the distribution); L_c mean, mean track length after c-axis correction using HeFTy (Ketcham et al. 2009), n D_{par}, number of etch pit diameters measured; D_{par} mean, mean etch pit diameter; n.d., not determined

(during α-disintegration of ^{238}U, ^{235}U, ^{232}Th and ^{147}Sm), which diffuses out of the mineral at a rate determined by the temperature and the He diffusivity of the mineral (Farley 2000, 2002; Reiners and Brandon 2006).

The closure temperature of the apatite He system in general is ~70 °C (cooling rate of 10 °C/Ma), for subgrain domain sizes >60 µm (Farley 2000), with larger crystals having a higher closure temperature (Farley 2000; Reiners and Farley 2001). For the zircon He system, the closure temperature is ~180 °C (Reiners et al. 2002, 2004). The partial retention zone (PRZ), the temperature range where the decay products are only partially retained, depends on the cooling rates (Reiners and Brandon 2006) and was adjusted repeatedly (e.g. Wolf et al. 1998; Flowers et al. 2009). Depending on the accumulated radiation damage in the crystal, the HePRZ in apatite can range from ~30 to 90 °C (Flowers et al. 2009). Also, for the zircon He system, radiation damage can have a great influence on the HePRZ, with closure temperatures increasing from ~140 to 220 °C, depending on the alpha doses (Guenthner et al. 2013).

Intra-sample age variation in He dating

Intra-sample age scatter in single-grain He ages can have various reasons (cf. Fitzgerald et al. 2006). In AHe data, complicating factors can be the presence of U- and Th-rich (micro)inclusions or He-rich fluid inclusions (Vermeesch et al. 2007), variations in crystal size (Reiners and Farley 2001), effects due to α-particle implantation (Spiegel et al. 2009) and/or ejection or any effects due to α-particle correction (Farley et al. 1996) or crystal zonation (Hourigan et al. 2005). In samples of this study, no zonation was apparent under the microscope, but cannot be excluded entirely and may in part account for the age scatter. Some samples show a correlation between crystal size and single-grain ages (cf. Chapter 4.2). Another factor causing scattered He ages is associated with varied He retentivity due to radiation damage (Green et al. 2006; Shuster et al. 2006; Flowers et al. 2006, 2009; Shuster and Farley 2009). The eU factor (effective Uranium concentration) was introduced (Shuster et al. 2006) to account for the dependency of ^4He diffusion on the amount of accumulated crystal defects created by alpha-recoil in the crystal lattice. Radiation damage-influenced samples commonly show a positive age–eU correlation (single-grain age vs. eU concentration) and can provide valuable information on their thermal history (Flowers 2009; Ault et al. 2013).

For ZHe analysis, the effects of radiation damage strongly depend on the eU concentrations (cf. Reiners et al. 2004; Reiners 2005; Guenthner et al. 2013). As discussed later, samples from the Albertine area show a critical eU threshold of ~600 µg/g. With increasing eU concentrations, an age–eU correlation is apparent. Therefore, we place most emphasis on ZHe ages of grains with eU < 600 µg/g. For the AHe data, minimum reproducible single-grain ages were considered as most reliable if no age–eU correlation is apparent. In these cases, we refer to the younger AHe single-grain ages, as apatite crystals from the Albertine area are often rich in inclusions, and undetected U- and Th-rich microinclusions are considered to be the prevailing complicating factors, leading to anomalously old AHe ages due to excess He.

Thermal history modelling

Thermal history modelling was performed using HeFTy v1.8.0 (Ketcham 2005). HeFTy provides a tool for testing geological models of time–temperature (t–T) evolution against a thermochronological data set, executing both forward and inverse model approaches. Geological constraints

Table 3 Apatite (U–Th–Sm)/He data of samples from Eastern D.R. Congo, western Albertine Rift

Sample Lab-no.	MWAR (μm)	U (μg/g)	Th (μg/g)	Sm (μg/g)	^{4}He (nmol/g)	eU (μg/g)	Ft	Raw age (Ma)	1σ (Ma)	Corr age (Ma)	1σ (Ma)
Southern area/West of Rwenzori											
DRC09-01-a1	36	3	7	80	2.2	5	0.62	93.8	23.1	151.3	37.2
DRC09-01-a2	51	3	4	65	1.7	5	0.71	68.5	7.4	95.8	10.4
DRC09-01-a3	43	14	6	171	12.5	17	0.70	142.1	7.2	203.0	10.3
DRC09-03-a1	52	26	31	128	13.8	34	0.74	76.4	1.5	102.8	2.0
DRC09-03-a2	86	16	17	57	12.8	20	0.82	117.6	2.4	143.4	2.9
DRC09-03-a3	50	14	12	55	9.8	17	0.70	108.2	4.6	154.4	6.5
DRC09-04-a1	39	23	40	138	18.7	33	0.65	105.9	3.3	163.5	5.1
DRC09-04-a2	*52*	*16*	*13*	*52*	*19.4*	*19*	*0.73*	*184.1*	*5.2*	*253.3*	*7.1*
DRC09-04-a3	47	14	12	58	9.4	17	0.71	104.2	4.7	146.2	6.6
DRC09-04-a4	42	11	8	41	9.5	14	0.68	129.9	6.7	191.3	9.8
DRC09-07-a1	69	4	2	116	1.5	5	0.77	65.3	4.7	85.0	6.1
DRC09-07-a2	63	9	3	198	6.0	11	0.76	112.6	4.5	148.4	6.0
DRC09-07-a3	54	20	3	210	11.2	22	0.73	96.9	2.8	132.2	3.9
DRC09-11-a1	77	11	1	266	4.6	13	0.81	72.7	1.7	89.7	2.1
DRC09-11-a2	73	15	4	280	6.9	18	0.80	76.0	1.6	95.3	2.1
DRC09-11-a3	51	12	7	280	6.0	15	0.75	80.3	2.6	107.5	3.5
DRC09-11-a4	35	21	5	127	7.8	23	0.66	64.0	2.3	96.4	3.5
DRC09-15-a1	*58*	*3*	*9*	*140*	*6.8*	*5*	*0.75*	*253.3*	*13.9*	*337.9*	*18.6*
DRC09-15-a2	48	2	8	120	1.0	5	0.69	46.8	6.5	67.7	9.4
DRC09-15-a3	*41*	*2*	*8*	*133*	*3.7*	*5*	*0.66*	*151.1*	*32.9*	*228.1*	*49.6*
DRC09-17-a1	*46*	*1*	*7*	*175*	*3.5*	*4*	*0.70*	*210.4*	*44.4*	*302.3*	*63.8*
DRC09-17-a2	42	5	26	170	7.2	12	0.68	116.4	7.5	171.6	11.0
DRC09-17-a3	*54*	*1*	*10*	*176*	*4.2*	*4*	*0.73*	*213.4*	*19.4*	*294.3*	*26.7*
DRC09-19-a1	56	4	13	144	2.5	7	0.74	66.9	3.2	90.6	4.3
DRC09-19-a2	48	0	1	145	0.2	1	0.68	67.3	80.3	99.0	118.2
DRC09-19-a3	54	1	3	198	0.8	3	0.74	74.1	17.5	100.7	23.7
DRC09-22-a1	*56*	*4*	*4*	*268*	*13.7*	*7*	*0.74*	*436.3*	*30.8*	*590.1*	*41.6*
DRC09-22-a2	46	9	4	216	6.6	12	0.71	112.7	5.5	159.3	7.8
DRC09-22-a3	55	6	4	271	2.7	8	0.73	74.3	5.1	101.8	7.0
DRC09-22-a4	56	6	5	250	3.9	8	0.75	100.0	4.6	133.4	6.2
Northern area/West of Lake Albert											
DRC09-29-a1	35	3	10	60	1.7	6	0.61	56.7	11.7	93.1	19.2
DRC09-29-a2	31	4	8	92	1.9	7	0.58	55.9	20.4	96.5	35.1
DRC09-29-a3	36	3	6	68	0.7	4	0.64	34.9	10.4	54.7	16.4
DRC09-30-a1	*36*	*1*	*2*	*11*	*0.9*	*2*	*0.64*	*102.4*	*59.1*	*160.8*	*92.9*
DRC09-30-a2	40	1	11	34	0.8	3	0.65	46.1	12.0	70.7	18.3
DRC09-30-a3	*49*	*35*	*50*	*117*	*56.9*	*47*	*0.72*	*221.6*	*4.4*	*305.8*	*6.0*
DRC09-34-a1	33	10	25	77	12.5	16	0.61	143.5	11.8	233.7	19.2
DRC09-34-a2	31	6	27	179	5.2	13	0.56	77.6	11.1	138.6	19.8
DRC09-34-a3	33	4	18	191	3.4	10	0.60	70.7	13.1	118.3	21.9
DRC09-36-a1	43	5	24	110	6.0	11	0.67	101.5	6.1	151.6	9.1
DRC09-36-a2	32	2	6	50	1.3	3	0.57	78.5	40.3	137.1	70.3
DRC09-36-a3	40	2	7	65	1.6	4	0.65	87.0	19.0	133.0	29.0
DRC09-36-a4	44	2	4	75	1.8	3	0.70	103.3	20.7	148.0	29.6
DRC09-36-a5	41	4	8	112	1.6	6	0.68	52.2	4.5	76.3	6.6
DRC09-37-a1	41	2	6	77	2.0	4	0.68	109.1	23.6	161.0	34.9
DRC09-37-a2	44	6	3	87	5.4	7	0.71	149.3	11.5	208.9	16.1

Table 3 continued

Sample Lab-no.	MWAR (μm)	U (μg/g)	Th (μg/g)	Sm (μg/g)	^{4}He (nmol/g)	eU (μg/g)	Ft	Raw age (Ma)	1σ (Ma)	Corr age (Ma)	1σ (Ma)
DRC09-37-a3	30	3	8	76	2.5	6	0.58	87.6	19.5	149.9	33.4
DRC09-37-a4	48	2	6	90	1.7	4	0.71	90.0	11.0	127.2	15.5
DRC09-41-a1	49	2	3	38	1.0	3	0.71	74.6	14.1	104.7	19.7
DRC09-41-a2	95	2	5	91	1.4	3	0.85	83.4	2.7	98.7	3.2
DRC09-41-a3	61	2	4	35	1.7	3	0.76	95.8	12.0	125.9	15.7

Provided are raw and corrected AHe ages with 1σ-analytical standard error; MWAR = mass-weighted average radius of aliquot; eU: effective uranium concentration (eU = [U] + 0.235[Th] + 0.0053[Sm], concentrations in wt %; after Spiegel et al. 2009); Ft: α-ejection correction factor. In italic, samples that are excluded from interpretation due to very low He content or probable excess He. For location and lithology, see Table 1

can be implemented as t–T constraints (t–T constraint boxes). Possible cooling history solutions are generated and provided as t–T paths (good and acceptable) that best approximate the thermochronological data set (for details see Ketcham et al. 2009; Ketcham 2013).

For this study, AFT data (single-grain cooling ages, *c*-axes-corrected track lengths, D_{par}) were modelled together with AHe and ZHe data (if available) using the multi-kinetic annealing model of Ketcham et al. (2007). To compute He diffusion, we used the diffusion models of Flowers et al. (2009) and Guenthner et al. (2013) to account for radiation damage. As constraints, we used information from AHe and ZHe dating. We started with wide constraint boxes and approached the AHe, AFT, ZHe closure temperatures. Two general geological evolution models were tested: (1) assuming a steady cooling only history and (2) allowing for reheating and cooling.

Exhumation rates can be assessed from t–T models, assuming surface temperature and geothermal gradient. The present-day surface temperature (Ts) was set to 20 ± 5 °C, representing the annual mean, and a geothermal gradient of 25 ± 5 °C/km was assumed. Albaric et al. (2009) derived a geothermal gradient of ~30 °C/km for the northern part of the western branch of the EARS, based on heat flow values ≥ 70 mW/m^2 and thermal conductivity values of 2.5 W/m K. For the Rwenzori area, Tugume and Nyblade (2009) determined heat flow values between 54 and 66 mW/m^2, i.e. consistent with average heat flow from Proterozoic terrains globally. Own conductivity measurements on rocks from the Rwenzori area (A. Foerster, GFZ Potsdam) revealed values of ~3 W/m K. Results from U–Pb thermochronometry also imply low cooling rates and a lower geothermal gradient (MacPhee 2006). Thus, an average geothermal gradient of about 25 ± 5 °C/km seems reasonable.

To evaluate the influence of the surface temperature on subsurface temperatures, i.e. the position of the isotherms, we used the 1D and 2D thermal history calculations of TERRA (Ehlers et al. 2005). Basic parameters such as diffusivity, basal temperature gradient and density of the crust were always kept the same. In order to develop an intuition for crustal thermal processes, we explored different erosion/exhumation scenarios and their influence on subsurface temperatures. Therefore, we tested different rates and durations of erosion by changing surface temperature, erosion rate, surface temperate laps rate and holding time. For details on the software, see Ehlers et al. (2005).

Results: low-temperature thermochronology data of the western rift shoulder

Apatite fission-track data

All AFT ages are reported as central age (±1σ) and range from 184 ± 14 to 608 ± 62 Ma (Fig. 2; Table 1). Apart from the sandstone sample DRC09-46, all samples are of igneous or metamorphic origin, with AFT ages younger than the corresponding intrusion or metamorphic ages. The AFT age of the sandstone sample is 385 ± 60 Ma, which is older than the assigned stratigraphic Permian age (Lepersonne 1974).

The youngest AFT age comes from a gneiss east of Butembo, located close to a NE–SW striking fault (Fig. 2). The sample sites of the two oldest ages are more than 150 km away from each other. Sample DRC09-22 (508 ± 26 Ma), a granite-gneiss, was taken from a downfaulted basement block, now located in the rift valley. The granite sample DRC09-34 (608 ± 62) is from the Blue Mountains in the northern part of the working area (Fig. 2). The remaining samples from the N–S transect range from 310 ± 24 to 356 ± 18 Ma.

Three of the AFT samples yielded at least 60 confined spontaneous fission-track lengths. Mean confined track (CT) length distributions range from 8.0 ± 0.6 to 11.3 ± 2.4 μm (Table 2). Measured confined tracks were corrected for their crystallographic orientation using the software HeFTy (Donelick et al. 1999; Ketcham et al. 2009). Resulting *c*-axis-corrected mean confined track length (L_c) distributions range from 11.3 ± 0.8 to 12.7 ± 2.0 μm. Most of them show a negative skewness (−0.10 to −1.34), with a tail of short tracks.

For all apatite grains used in this study, a total of 1,026 D_{par} values (etch pit size) were determined (Table 2). Mean D_{par} values range from 1.1 ± 0.3 µm, indicative for F-rich apatite, to 2.3 ± 0.4 µm, indicative for Cl-rich apatite. Most samples show positively skewed D_{par} distributions, with the determined D_{par} values pointing towards a dominance of fluorapatite in the dated grains. Large skewness values indicate greater variations in D_{par}. In some samples, a subtle positive correlation between single-grain AFT cooling ages and corresponding D_{par} is evident (Appendix Fig. A1), indicating varying annealing kinetics of single grains within one sample. This accounts for sample DRC09-36 with a low value for the Chi-square (χ^2) statistics test and can also cause AFT results to fail the test. An accumulation of high U single-grain ages with small errors can also cause a sample to fail the Chi-square test, while the sandstone sample with mainly low U concentrations passes the test despite a broad range of single-grain ages (Fig. 2).

Apatite and zircon (U–Th–Sm)/He data

Apatite (U–Th–Sm)/He analyses (AHe dating) were performed on 15 samples, with 3–4 single-grain measurements for each sample (Table 3; Fig. 2). Corrected single-grain ages (±1σ) range from 590 ± 42 to 55 ± 16 Ma, with very low U concentrations for some samples. The higher single-grain ages of samples DRC09-04 and DRC09-15 seem to correlate with increasing grain size (Fig. 5). In some samples, a positive correlation between single-grain AHe ages and eU concentration is apparent (Fig. 5). A similar trend was detected in samples from the adjacent Rwenzori Mtns (Bauer et al. 2013). Scattered single-grain AHe ages are ascribed to undetected U- and Th-rich microinclusions, grain size variations and accumulated radiation damage due to a prolonged cooling history (Green et al. 2006; Flowers et al. 2009). Outlier single-grain ages due to very low He concentrations or microinclusions (“parent-less” He) are excluded from further interpretation as there is no control on the factor that caused the scatter. Samples that show a correlation between single-grain age and radiation damage (Fig. 5) are used to further constrain the cooling history (Shuster et al. 2006; Flowers et al. 2009). Considering the effects of radiation damage can also explain apatite suites with AHe ages that are older than the corresponding AFT age (Flowers et al. 2009), e.g. sample DRC09-04.

ZHe dating was carried out on 14 samples, with 3–4 single grains analysed for each sample. Corrected single-grain ages (±1σ) range from 1,086 ± 18 to 20 ± 0.3 Ma (Table 4; Fig. 2). The young age is from sample DRC09-17, which shows a wide spread in cooling ages and most likely is affected by radiation damage with eU concentrations above 1,600 µg/g. Most of the corrected ZHe ages with moderate eU concentrations are in the range of 321 ± 5 to 531 ± 11 Ma. About half of the analysed zircon grains have high U and Th concentrations and corresponding high eU contents. The amount of radiation damage and the cooling history of the host rock bias the ZHe diffusivity: it can either decrease when He is trapped, or it can increase as numerous traps are connected (Guenthner et al. 2013). Radiation damage in zircons can therefore result in either older or younger cooling ages (Reiners et al. 2004; Farley 2007; Guenthner et al. 2013). For the Rwenzori area, a critical threshold of ~600 µg/g for eU concentration was determined (Bauer et al. 2013). This seems applicable also for the samples from the western rift shoulder of the Albertine Rift and can explain LTT age patterns with ZHe ages younger than the corresponding AFT ages. Grains below this critical threshold (eU < 600 µg/g) are considered to most reliably yield effective closure temperatures close to the expected 180–200 °C.

Thermal modelling

Individual thermal history simulations were carried out for 6 samples using HeFTy. The robustness of thermal modelling (t–T evolution) strongly depends on the amount of detected confined track lengths. Therefore, three of the modelled samples with less than 60 confined track lengths were taken for comparison only. From the different t–T model scenarios tested (steady cooling only and reheating), a reheating scenario is feasible for samples DRC09-07 and DRC09-37 (Fig. 6).

The general cooling pattern of the samples from the western rift shoulder indicates a prolonged cooling history with a first phase of accelerated cooling in Palaeozoic times, followed by slow constant cooling and a slightly accelerated cooling in Palaeogene to Neogene times. In part, a moderate Mesozoic reheating was observed with a temperature increase of ~40 °C (Fig. 6).

Discussion

One of the main conclusions of previous work on the thermal evolution of the Rwenzoris was that exhumation was not solely triggered by Neogene rifting (Bauer et al. 2010b, 2013). Instead, they show a protracted exhumation history. Taking the new data from the western rift shoulder into account, a more comprehensive picture of the thermal and geodynamic evolution of the Albertine Rift can be drawn.

The LTT results from the western rift shoulder of the Albertine Rift in the DRC also reveal cooling ages that are older than expected for a Neogene to recent rift environment. Cooling histories point to a protracted cooling of the western rift shoulder with an initial cooling event

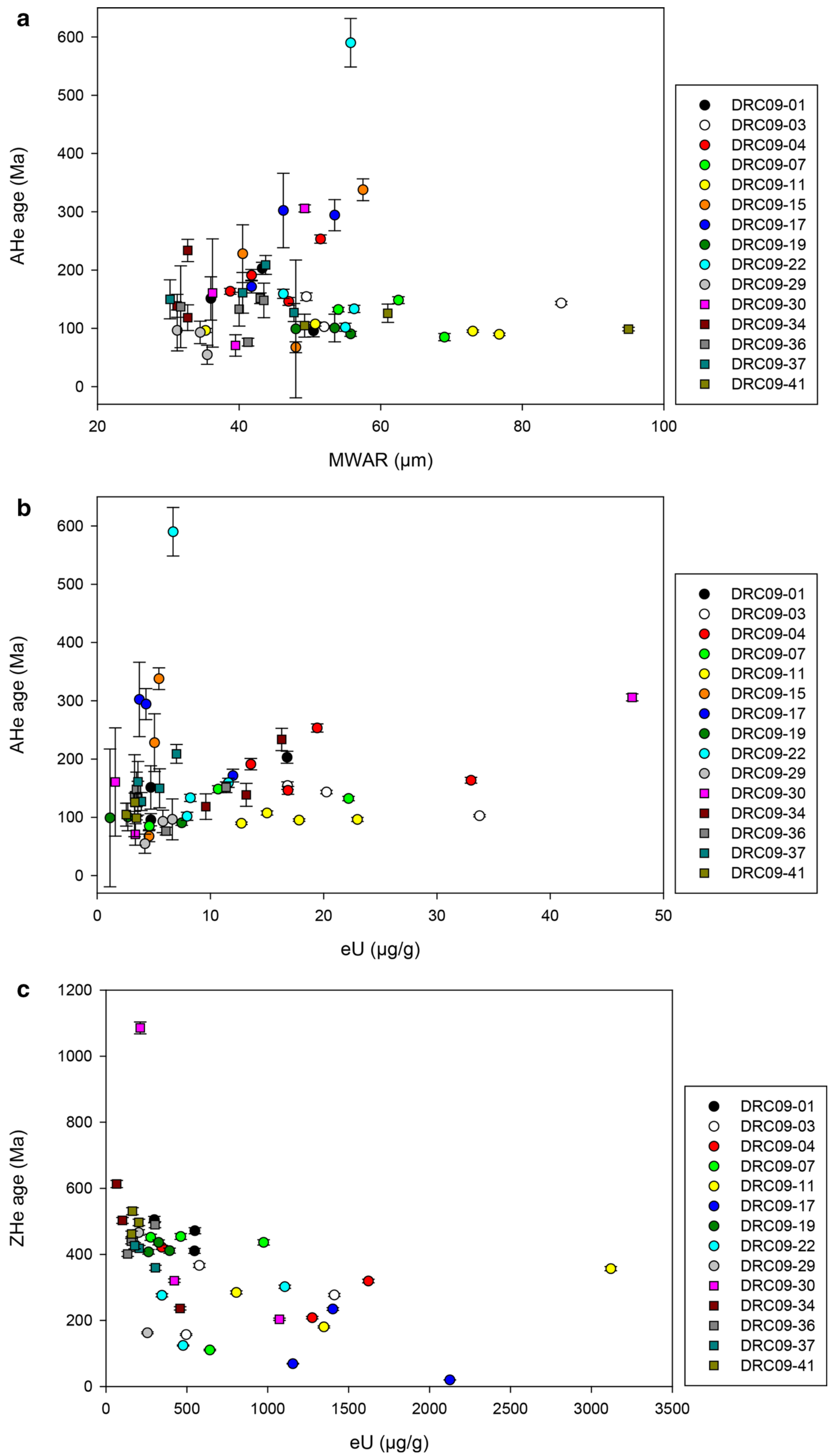

Fig. 5 AHe single-grain (±1σ) ages plotted against **a** grain size; **b** eU concentration; some samples, e.g. DRC09-01 and DRC09-34, show a clear correlation between single-grain ages and eU concentration. Evaluation of dependencies allows deciphering outliers, e.g. oldest AHe single-grain age of DRC09-22; **c** ZHe single-grain ages (±1σ) plotted against eU; most samples show a dependency between single-grain ages and eU above a critical eU concentration threshold of ~600 µg/g, with either positive or negative correlation or both. Uncertainties in part below marker size

in mid-Palaeozoic times. The overall erosion of the western rift shoulder since initial Palaeozoic cooling, derived from the AFT data, is below 5 km. The erosion rates for the Neogene rifting episode are low (<0.1 km/Ma) and do not reflect intensified erosion commonly associated with a rift setting (Roberts and Yielding 1991; van der Beek et al.

Table 4 Zircon (U–Th)/He data of samples from Eastern D.R. Congo, western Albertine Rift

Sample Lab-no.	MWAR (µm)	U (µg/g)	Th (µg/g)	^{4}He (nmol/g)	eU (µg/g)	Ft	Raw age (Ma)	1σ (Ma)	Corr age (Ma)	1σ (Ma)
Southern area/West of Rwenzori										
DRC09-01-zr1	38	478	302	1,054.1	549	0.73	345.7	6.8	471.7	9.3
DRC09-01-zr2	36	258	173	607.9	299	0.72	365.8	7.1	505.3	9.9
DRC09-01-zr3	36	460	372	909.4	547	0.73	300.5	5.6	410.6	7.6
DRC09-03-zr1	*39*	*1,161*	*1,064*	*1,573.5*	*1,411*	*0.73*	*203.3*	*3.3*	*277.0*	*4.6*
DRC09-03-zr2	41	502	316	890.1	576	0.76	279.6	4.6	366.5	6.1
DRC09-03-zr3	38	452	184	316.6	495	0.75	117.4	1.9	157.3	2.6
DRC09-04-zr1	43	1,522	423	2,207.6	1,622	0.77	247.0	4.3	319.3	5.5
DRC09-04-zr2	48	1,166	461	1,121.9	1,274	0.77	161.0	2.8	208.4	3.6
DRC09-04-zr3	37	249	407	579.5	345	0.72	304.3	4.5	421.5	6.3
DRC09-07-zr1	45	254	94	534.7	276	0.77	348.4	7.1	451.5	9.3
DRC09-07-zr2	41	427	150	870.9	462	0.75	339.3	6.7	454.2	8.9
DRC09-07-zr3	50	535	455	306.8	642	0.80	88.0	1.6	110.5	2.0
DRC09-07-zr4	45	904	297	1,805.0	974	0.76	333.6	6.2	436.4	8.1
DRC09-11-zr1	47	1,194	649	1,029.6	1,346	0.78	140.2	2.3	180.4	2.9
DRC09-11-zr2	47	2,872	1,052	4,761.1	3,119	0.77	276.3	4.7	356.8	6.1
DRC09-11-zr3	41	716	378	949.2	805	0.75	214.6	3.5	284.9	4.6
DRC09-17-zr1	*26*	*884*	*1,151*	*276.7*	*1,155*	*0.64*	*44.2*	*0.7*	*69.0*	*1.0*
DRC09-17-zr2	*32*	*1,319*	*352*	*1,242.5*	*1,402*	*0.69*	*162.1*	*2.8*	*234.6*	*4.1*
DRC09-17-zr3	*27*	*1,670*	*1,937*	*148.2*	*2,125*	*0.65*	*12.9*	*0.2*	*20.0*	*0.3*
DRC09-19-zr1	48	219	187	464.2	263	0.78	318.5	5.5	407.6	7.0
DRC09-19-zr2	48	337	239	701.0	393	0.78	321.7	6.0	411.4	7.6
DRC09-19-zr3	42	273	223	599.5	325	0.76	332.1	5.8	436.3	7.6
DRC09-22-zr1	31	321	103	365.2	345	0.70	192.8	3.4	276.2	4.8
DRC09-22-zr2	34	978	540	1,342.4	1,105	0.73	221.1	3.6	302.1	5.0
DRC09-22-zr3	45	341	577	245.4	476	0.76	94.7	1.3	124.2	1.8
Northern area/West of Lake Albert										
DRC09-29-zr1	66	228	119	193.0	256	0.85	138.1	2.3	162.7	2.7
DRC09-29-zr2	64	151	58	345.1	165	0.84	375.1	6.5	447.9	7.7
DRC09-29-zr3	62	186	70	439.9	202	0.84	389.9	7.1	466.3	8.5
DRC09-30-zr1	35	376	200	524.3	423	0.70	225.6	3.8	320.4	5.4
DRC09-30-zr2	31	951	515	806.1	1,072	0.68	137.9	2.4	203.6	3.5
DRC09-30-zr3	*29*	*164*	*200*	*865.5*	*211*	*0.66*	*715.0*	*11.9*	*1,085.5*	*18.1*
DRC09-34-zr1	46	89	55	224.9	102	0.79	394.9	7.0	502.9	9.0
DRC09-34-zr2	53	57	39	182.6	66	0.80	490.4	8.6	613.1	10.7
DRC09-34-zr3	53	405	226	473.3	458	0.80	188.6	3.9	236.5	4.9
DRC09-36-zr1	41	137	89	289.6	157	0.75	331.6	6.2	439.9	8.3
DRC09-36-zr2	46	118	69	230.0	134	0.77	309.8	5.9	401.4	7.6
DRC09-36-zr3	40	276	114	619.9	303	0.75	367.9	6.6	489.8	8.8
DRC09-37-zr1	43	278	118	466.9	305	0.77	276.7	5.9	359.4	7.6
DRC09-37-zr2	47	178	116	374.3	205	0.79	328.7	7.0	418.3	8.8
DRC09-37-zr3	43	161	72	322.9	178	0.77	327.5	7.3	426.2	9.5
DRC09-41-zr1	37	146	54	292.8	158	0.72	332.9	6.3	461.8	8.8
DRC09-41-zr2	36	143	87	354.8	163	0.73	389.5	7.7	530.8	10.5
DRC09-41-zr3	36	179	102	406.8	203	0.72	359.6	7.1	496.9	9.8

Provided are raw and corrected ZHe ages with 1σ-analytical standard error; MWAR = mass-weighted average radius of aliquot; eU: effective uranium concentration (eU = [U] + 0.235[Th], concentrations in wt %, after Shuster et al. 2006); Ft: α-ejection correction factor. In italic, samples that are excluded from interpretation due to extreme high non-replicable 1σ standard deviation. For location and lithology, see Table 1

1994). Linking the results from LTT and thermal history modelling from the western rift shoulder with the geological and morphological constraints of the working area, requires to link (1) "old" cooling ages, (2) a protracted cooling history and (3) low erosion rates with Cenozoic rifting and a high topographic relief.

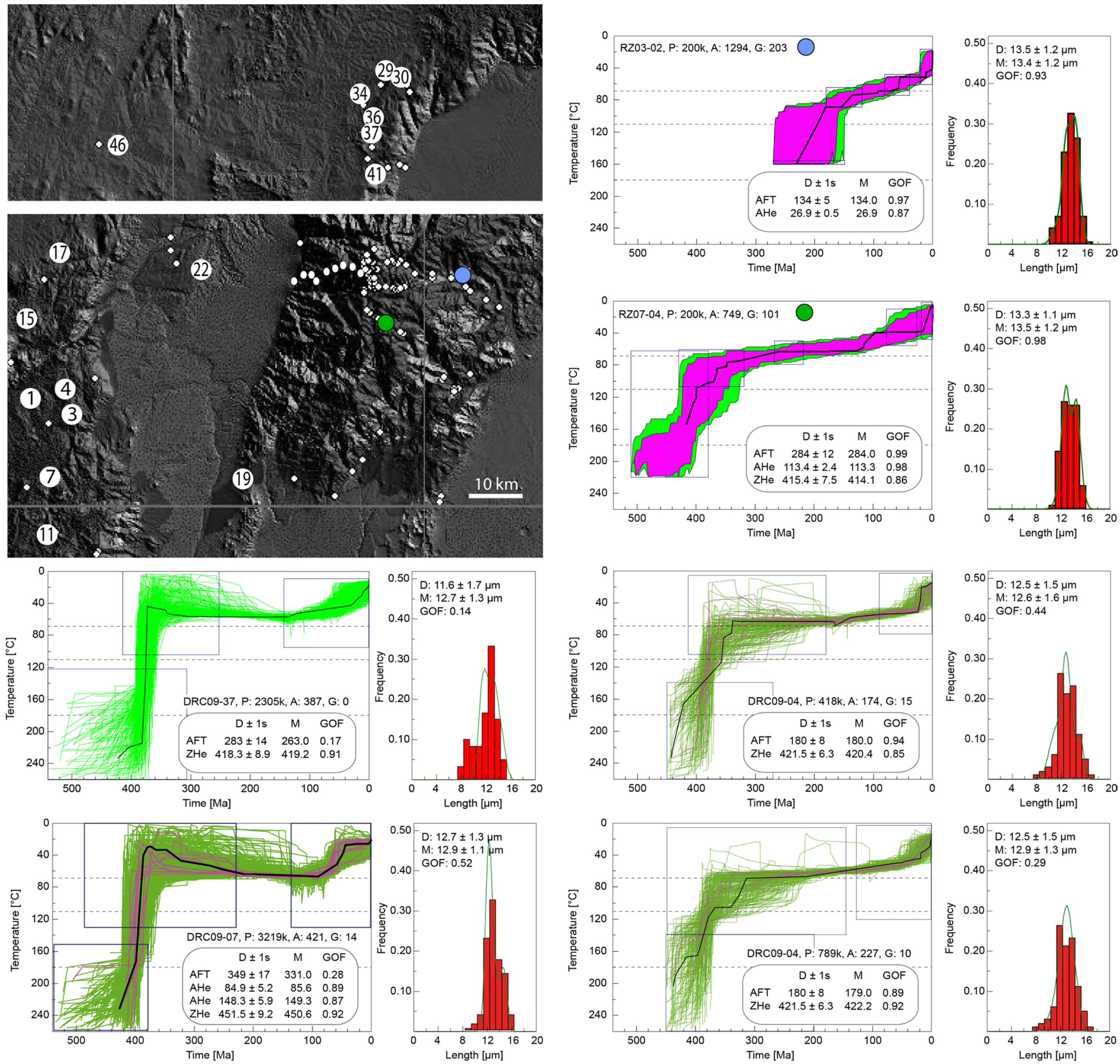

Fig. 6 Results from inverse thermal history modelling using HeFTy (Ketcham et al. 2009). Representative t–T paths illustrate the cooling history of samples from the western rift shoulder and the central Rwenzoris for comparison. In the central Rwenzoris, a northern (AFT cooling ages scatter ~130 Ma) and southern block (AFT cooling ages scatter ~300 Ma) are distinguished. Displayed are envelopes of t–T paths for samples from the Rwenzoris (RZ) and t–T paths for samples from the western rift shoulder (DRC), with *c*-axes-corrected confined fission-track length (CT) frequency distribution overlain by calculated probability density function (best fit). Sample locations are shown in the DEM. Prolonged and differentiated cooling is obvious from all samples. Samples from the western rift shoulder and the southern block (*green*) show earlier onset of cooling. Samples from the northern block (NB) show cooling through the 110 °C isotherm much later; see text for more details. HeFTy models: *P* paths tried, *A* acceptable fit models (*green* paths), *G* good fit models (*pink* paths), *D* determined AFT, AHe, ZHe age (1σ), CT, *M* modelled AFT, AHe, ZHe age, and CT, *G.O.F.* goodness of fit

"Old" cooling ages

Results from ZHe, AFT and AHe analyses reveal old cooling ages for the western rift shoulder (Fig. 2), similar to samples from the southern block of the central Rwenzori Mtns and the eastern rift shoulder of the Albertine Rift (cf. Fig. 4 and Bauer et al. 2010b, 2013). Most ZHe ages of the western rift shoulder indicate cooling below ~180 °C during Ordovician to Silurian times. Exceptions are mainly related to samples with high eU concentrations, resulting in potentially unreliable cooling ages. The majority of the AFT data show Devonian to Carboniferous ages (310 ± 24 to 356 ± 18 Ma). This indicates that the rocks resided in a near-surface position (~3–4 km) since mid-Palaeozoic times. Most of the AFT data reveal cooling below ~110 °C in the Carboniferous. If the old AFT ages of samples DRC09-22 (508 ± 28 Ma, from a down-faulted block) and DRC09-34 (608 ± 62 Ma, from the Blue Mountains) do not reflect anomalous closure temperatures due to unusual chemical compositions, those rocks must have cooled below ~110 °C in Neoproterozoic to Cambrian times. They could represent distinct blocks with very little exhumation since Pan-African times. Forming small topographic highs, these rocks might have been protected from severe erosion or burial. Taking into account that in both cases the AFT and ZHe ages are inverted requires further analyses in order to interpret these ages properly. The Jurassic AFT sample (DRC09-04: 184 ± 14 Ma) can be explained by fault-related movements with intensified erosion. It is located in the area of Butembo and has the highest altitude of all AFT samples (Table 1; Fig. 2b). In this area, several ~WSW-ENE faults were observed, similar to a prominent fault strike in the Rwenzori Mtns (Fig. 2). This age might reflect footwall cooling related to Jurassic normal faulting as also described for the central Rwenzori Mtns (Bauer et al. 2010b). Enhanced advection along the fault and a localized thermal overprint could be another explanation. AHe cooling ages of the same sample are only slightly younger, supporting a localized thermal overprint. Single-grain AHe ages from the western rift shoulder mainly scatter around 150 Ma, indicating cooling below ~70 °C in the late Jurassic to early Cretaceous. The younger AHe single-grain ages of late Cretaceous to Palaeocene age (55 ± 16 to 85 ± 6 Ma) might record a moderate burial below a thin sedimentary cover that was eroded in early Cenozoic times or a short-term slight increase in the geothermal gradient. Burial seems more likely, as this would allow for the more locally distributed younger AHe ages. Assuming a hilly area at that time, the sedimentary cover could have experienced locally variable transit times with either brief or prolonged periods of storage before being eroded again. This would result in locally variable short-termed reheating, capable of affecting the sensitive AHe system.

Protracted cooling history of the western rift shoulder

The samples from the western rift shoulder predominantly reveal negatively skewed track length distributions, with a tail of short tracks, indicating a complex cooling history (Table 2). Samples with a sufficient number of confined fission-tracks for thermal history modelling show a consistent overall cooling pattern: a first phase of accelerated cooling occurred at ~400 to 450 Ma and exhumed the rocks into the apatite partial annealing zone. After the Permo-Carboniferous, the rocks were exhumed gradually and extremely slowly for the following ~200 Ma with constant cooling rates to ~40 to 50 °C. HeFTy models suggest a moderate Mesozoic reheating episode with a temperature increase of ~40 °C. The final, slightly accelerated cooling period to surface temperatures was initiated in late Cretaceous to Palaeogene times, with exhumation to the present outcrop levels since ~40 Ma (Fig. 6). This is consistent with previous studies from the EARS and Madagascar, which also report Carboniferous to Permian AFT ages for basement rocks (Emmel et al. 2008; Bauer et al. 2013 and literature therein). Exceptions are the rocks from the northern Rwenzoris and the northern block of the central Rwenzoris. There, a Jurassic cooling phase can be observed, and the final cooling is slightly shifted to the Neogene. Cooling histories indicate that large parts of the Albertine Rift were "cold" by the end of the Mesozoic, i.e. rocks have passed the ~70 °C isotherm (Fig. 6), remaining with just minor overburden on top to be eroded.

Low erosion rates

AFT ages suggest less than 5 km of erosion since the Palaeozoic (2.8 to 4.8 km). The calculation assumes an average AFT closure temperature of 110 °C, a geothermal gradient of 25 ± 5 °C/km and a present-day surface temperature of 20 ± 5 °C. However, any transient sedimentary cover during this time span is not taken into account and might add another 1 to 2 km of erosion.

Based on thermal history models, a net erosion of 6.4 ± 1.3 km since Palaeozoic times (460 Ma) can be inferred, assuming that cooling is due to erosion only. Major cooling occurred during the first cooling event until ~400 Ma. Afterwards, erosion is limited to ~2 to 3 km (Table 5). This is confirmed by sandstone sample DRC09-46. Its ATF age (385 ± 60 Ma) is older than its depositional age (Permo-Carboniferous), reflecting cooling of the source area and no or minimal post-depositional thermal resetting. Thus, a maximum overburden of 3 to 4 km can be inferred. The AHe cooling ages (Tc: 70 °C) suggest a maximum erosion of ~1.5 to 2.8 km since the late Jurassic (~150 Ma). Locally, the timing can be shifted to late Cretaceous to Palaeocene times, considering the youngest AHe cooling ages (55 ± 16 to 85 ± 6 Ma). Neogene exhumation rates along the rift shoulder are in the order of 0.02 km/Ma. These low erosion rates are in agreement with rates from the Rwenzori Mtns (Roller et al. 2012; Bauer et al. 2013).

Cenozoic rifting

The Albertine rift shoulders reveal cooling ages and thermal histories that do not support continuous Neogene surface

Table 5 Exhumation rates for samples from Eastern D.R. Congo, western Albertine Rift

Sample	Cooling phase	t–t (Ma)			T–T (°C)			Cooling rate (°C/Ma)	Exhumation rates		
									(km/Ma)	(km/Ma)	(km/Ma)
		*t*1	*t*2	d*t*	*T*1	*T*2	d*T*		(20 °C/km)	(25 °C/km)	(30 °C/km)
DRC-09-04	1	440	400	40	180	90	90	2.250	0.113	0.090	0.075
DRC-09-04	2	400	40	180	80	55	25	0.139	0.007	0.006	0.005
DRC-09-04	3	40	0	40	55	20	35	0.875	0.044	0.035	0.029
DRC-09-07	1	460	440	20	180	90	90	4.500	0.225	0.180	0.150
DRC-09-07	2	440	400	40	90	45	45	1.125	0.056	0.045	0.038
DRC-09-07	*3a*	*400*	*100*	*300*	*45*	*60*	*−15*	*−0.050*	*−0.003*	*−0.002*	*−0.002*
DRC-09-07	3b	100	60	40	60	35	25	0.625	0.031	0.025	0.021
DRC-09-07	4	60	0	60	35	20	15	0.250	0.013	0.010	0.008
DRC-09-37	1	430	410	20	180	80	100	5.000	0.250	0.200	0.167
DRC-09-37	2	410	400	10	80	55	25	2.500	0.125	0.100	0.083
DRC-09-37	*3a*	*400*	*140*	*260*	*55*	*65*	*−10*	*−0.038*	*−0.002*	*−0.002*	*−0.001*
DRC-09-37	3b	140	60	80	65	45	20	0.250	0.013	0.010	0.008
DRC-09-37	4	60	0	60	45	20	25	0.417	0.021	0.017	0.014

Cooling phases and time–temperature information were derived from HeFTy model solutions using mean time–temperature paths. Exhumation rates were calculated considering cooling rate, surface temperature and geothermal gradients of 25 ± 5 °C/km; t–t: time segment; T–T: Temperature segment. In italic phases with reheating

uplift and associated erosion up to several kilometres as known from other rift environments (Burov and Cloetingh 1997). Maximum Neogene erosion rates determined for the western rift shoulder are ~0.02 km/Ma (Table 5), with the eastern and western rift shoulders in parts covered by more than 30 m of laterite. Cooling histories and the AHe age distribution indicate that the rift shoulder was "cold" (<70 °C) since about 70 Ma. Thus, erosion of the rift shoulder associated with rift flank surface uplift was much lower than expected from common tectonic models of rift faulting (Kusznir and Ziegler 1992; Burov and Cloetingh 1997). Similar results of slow erosion of rift shoulders have been reported for the Malawi and Rukwa rift with an estimated erosional denudation of the escarpment <200 m (van der Beek et al. 1998). Further examples of rift flanks with unexpectedly old cooling ages and associated low exhumation rates can be found along the Brazilian South Atlantic margin (Karl et al. 2013). Thus, the low erosion rates along the flanks of the Albertine Rift and the deviation from common rift models is attributed to the fact that different parameters such as basement fabrics, rift style, lithospheric composition as well as climate highly affect the various rift environments and their landscape evolution.

"Palaeo-Cold Spot"

In Palaeozoic times, the African continent experienced several glaciations, with major glaciations in Ordovician and particularly in Permo-Carboniferous times (Fig. 4). Major cooling events in the Albertine area derived from time–temperature modelling seem to correlate with these phases of cooling.

The first cooling event in the Silurian/Devonian (>400 Ma) coincides with major glaciations in Gondwana. As part of Gondwana, the African plate had a southerly position, with the South Pole located in Northwest Africa during the late Ordovician (Guiraud et al. 2005). A strong global glaciation is registered for the latest Ordovician, followed by "gentle but widely registered tectonism" and deglaciation in the early Silurian (Guiraud et al. 2005). Late Palaeozoic Gondwana glaciations affected the continent starting at about 350 Ma and lasting for several tens of millions of years (Eyles 2008). Evidence of Carboniferous–Permian glaciations has been reported for areas as far north as Gabon, western Sudan and Somalia (Catuneanu et al. 2005), with remains also in Uganda and DRC (Cahen and Lepersonne 1981; Schlueter et al. 1993; Bradley et al. 2010). It is not clear how far south the Ordovician glaciations reached and how severe the influence of the Permo-Carboniferous glaciation was on the Albertine area. However, the old cooling ages of the western rift shoulder testify that these rocks had a near-surface position for a long time.

Neogene glaciation cycles in the Rwenzoris are linked to their high altitude. Associated glacial erosion is not deep enough and too recent to be recorded by the thermochronometers used. From detrital thermochronology, a Plio-Pleistocene exhumation phase with ~500 m of erosion was derived (Bauer et al. 2013), matching glacial landscape models and recent erosion rates of the Rwenzoris (Kaufmann and Romanov 2012; Roller et al. 2012).

Studies on glacial erosion rates from the Patagonian Andes and Greenland showed that glaciations can preserve landscapes and protect the underlying bedrock instead of eroding it (Thomson et al. 2010; Bierman et al. 2014). It was also shown that cold average temperatures during long-lasting glaciations prevail, despite waxing and waning of the ice shield (Lemke et al. 2007). To evaluate a possible influence of long-lasting cold surface temperatures on the position of the isotherms, we applied 1D and 2D thermal history calculations using TERRA (Ehlers et al. 2005). The modelling results show minor changes in the position of the isotherms that are within the error of the cooling ages. A direct influence on the geothermal gradient can therefore be neglected. Although the more sensitive AHe system may record cooling due to long-lasting very low surface temperatures, the main effect of the glaciations in this area was their eroding capacity.

The changes between hothouse and icehouse conditions since the Ordovician (Burgoyne et al. 2005) probably had a strong impact on weathering and subsequent erosion. The circumstance that several glaciations affected the Albertine area supports the assumption that overburden since the Palaeozoic was small. The few Palaeozoic sedimentary rocks from the margin of the Congo Basin (DRC09-46) confirm the presence of a sedimentary cover that persisted only in depressions and pockets where it was protected from erosion.

Long-term landscape evolution of the Albertine area

A plausible scenario describing the long-term landscape evolution and exhumation history of the Albertine Rift starts with the Palaeoproterozoic fold and thrust belt that structured the crust of the later Albertine Rift (Link et al. 2010). The Pan-African orogeny affected the Albertine area, causing movements along long-lived faults. Locally, individual basement blocks might have formed already then, like the down-faulted block of sample locality DRC09-22. The mid-Palaeozoic cooling provides a first traceable imprint on the exhumation history. It correlates with the ending of the Ordovician glaciation that shows an almost instantaneous change in climate (Burgoyne et al. 2005). This most likely resulted in intensified erosion that could have been triggered by minor rock and surface uplift due to far-field effects from shortening in northern Africa (Guiraud et al. 2005). In Carboniferous times, most of the sampled rocks reached a near-surface position in the uppermost crust, ~2.8 to 4.8 km below the surface. Throughout the Mesozoic, the area was tectonically stable with minor faulting and exhumation detected in the Rwenzori Mtns (MacPhee 2006; Bauer et al. 2010b, 2013). On the western rift shoulder, a similar trend can be observed, with cooling through the ~110 °C isotherm in the early Jurassic, which correlates with Karoo magmatic activity. Large parts of the area were slowly exhumed. A minor reheating in Jurassic to Cretaceous times could be the result of a short-term increase in the geothermal gradient or burial under a thin sedimentary cover. Burial would point to an area with some relief, where sediments were trapped and stored before being eroded again. The Albertine area could have acted as a source area for the Congo Basin, where thick sedimentary successions were deposited (Cahen et al. 1959; Kadima et al. 2011). After the predominantly stable Mesozoic phase, a period of slightly accelerated cooling occurred. This correlates with erosional cooling in the Rwenzori Mtns (Bauer et al. 2010b, 2013) and is associated with Cenozoic rifting in the western branch of the EARS. Exhumation rates of ~0.02 km/Ma indicate slow erosion that does no account for major erosion along the rift shoulder. This observation could support the hypothesis of an elevated Albertine area, where the Albertine Rift already formed a high plateau and the rift valley itself collapsed by down faulting. The associated rift shoulder uplift was not marked enough to exhume rocks with young cooling ages.

Conclusions

LTT data from the western rift shoulder of the Albertine Rift (DRC) show old cooling ages, up to early Palaeozoic. These old cooling ages and thereof derived protracted thermal history models point to a long residence time of the sampled rocks in the uppermost crust. Erosion rates of the western Albertine rift shoulder are low, indicating that the current surface was at or near the surface (< 4.8 km) since about Permo-Carboniferous times. The fact that known rifting models are not entirely applicable to this area results from influencing factors such as inherited basement fabrics, rift style, lithospheric composition and climate. Palaeozoic glaciations that affected the area likely enhanced erosion, preventing the accumulation of a thick sedimentary cover over a long time span. Associated weathering might have affected the basement allowing for subsequent erosion. Thermal history models point to an accelerated cooling/exhumation in Devonian times and minor Jurassic–Cretaceous reheating. This might be interpreted as a Mesozoic Albertine high that was slowly eroded, acting as a long-lasting source area for the Congo Basin.

Acknowledgments This study was funded by the DFG (Deutsche Forschungsgemeinschaft) through the research unit RiftLink (DFG research unit 703, GL 182/9-2). Further funding was provided by the DAAD (Deutscher Akademischer Austausch Dienst) through a short-term research stay grant. Field work was supported by the Ruwenzori State University in Butembo. We particularly thank Dr. Meni

Malikwisha and Bin V. Mutete, as well as Celestin Kasereka Mahinda from Goma Volcano Observatory. We also gratefully acknowledge the support given by the ICCN (Institut Congolais pour la Conservation de la Nature), the CEEC (Centre of Evaluation, Expertise and Certification) and the Ministry of Mining. We express our thanks to the governor of North-Kivu for supporting us during our expedition. We also thank the officials from Bunia and the Local Chiefs of the entire region for their support. Acknowledgement is also given to the RiftLink research group for thorough discussions, to Alexis Ault and Benjamin Emmel for very helpful reviews, to the editor, Dieter Mertz, and to Anna Ksienzyk for their support. We thank Peter W. Reiners and Uttam Chowdhury for analytical assistance and valuable discussions. ASTER GDEM, product of METI & NASA, and OneGeology is thanked for providing their material.

References

Aanyu K (2011) Implications of regional fault distribution and kinematics for the uplift of rift flanks around the Rwenzori mountains, Southwestern Uganda. Thesis, Johannes Gutenberg University Mainz

Aanyu K, Koehn D (2011) Influence of pre-existing fabrics on fault kinematics and rift geometry of interacting segments: analogue models based on the Albertine Rift (Uganda), Western Branch-East African Rift System. J Afr Earth Sci 59:168–184. doi:10.1016/j.jafrearsci.2010.10.003

Abbate E, Balestrieri ML, Bigazzi G (2002) Morphostructural development of the Eritrean rift flank (southern Red Sea) inferred from apatite fission track analysis. J Geophys Res 107:2319–2331

Albaric J, Déverchère J, Petit C, Perrot J, Le Gall B (2009) Crustal rheology and depth distribution of earthquakes: insights from the central and southern East African Rift System. Tectonophysics 468:28–41

Appel P, Schenk V, Schumann A (2005) P-T path and metamorphic ages of pelitic schists at Murchison Falls, NW Uganda: evidence for a Pan-African tectonometamorphic event in the Congo Craton. Eur J Mineral 17:655–664

Ault AK, Flowers RM, Bowring SA (2013) Phanerozoic surface history of the Slave craton. Tectonics 32:1066–1083. doi:10.1002/tect.20069

Badalini G, Redfern J, Carr ID (2002) A synthesis of current understanding of the structural evolution of North Africa. J Petrol Geol 25:249–258

Bahat D, Mohr P (1987) Horst faulting in continental rifts. Tectonophysics 141:61–73

Bauer FU, Glasmacher UA, Malikwisha M, Mambo VS, Mutete BV (2010a) The Eastern Congo—a beauty spot, rediscovered from a geological point of view. Geol Tod 26:55–64

Bauer FU, Glasmacher UA, Ring U, Schumann A, Nagudi B (2010b) Thermal and exhumation history of the central Rwenzori Mountains, Western Rift of the East African Rift System, Uganda. Int J Earth Sci 99:1575–1597. doi:10.1007/s00531-010-0549-7

Bauer FU, Karl M, Glasmacher UA, Nagudi B, Schumann A, Mroszewski L (2012) The Rwenzori Mountains of western Uganda—an approach to unravel the evolution of a remarkable morphological feature within the Albertine Rift. J Afr Earth Sci 73–74:44–56

Bauer FU, Glasmacher UA, Ring U, Karl M, Schumann A, Nagudi B (2013) Tracing the exhumation history of the Rwenzori Mountains, Albertine Rift, Uganda, using low-temperature thermochronology. Tectonophysics 599:8–28

Bierman PR, Corbett LB, Graly JA, Neumann TA, Lini A, Crosby BT, Rood DH (2014) Preservation of a preglacial landscape under the center of the Greenland Ice Sheet. Science 344:402–405

Bradley G, Carter A, Taylor RG (2010) Denudation history of Permo Carboniferous glacial strata and Precambrian basement on the East African Plateau adjacent to the Eastern Flank of the Western Rift. In: Thermo2010, 12th international conference on thermochronology, Glasgow, 16–20 August 2010

Bumby AJ, Guiraud R (2005) The geodynamic setting of the Phanerozoic basins of Africa. J Afr Earth Sci 43:1–12

Burgoyne PM, van Wyk AE, Anderson JM, Schrire BD (2005) Phanerozoic evolution of plants on the African plate. J Afr Earth Sci 43:13–52

Burke K, Macgregor DS, Cameron N (2003) African petroleum systems: four tectonic "aces" in the past 600 million years. In: Arthur TJ, Macgregor DS, Cameron NR (eds) Petroleum geology of Africa: new themes and developing technologies, vol 207. Geological Society, London, Special Publications, pp 21–60

Burov E, Cloetingh S (1997) Erosion and rift dynamics: new thermomechanical aspects of post-rift evolution of extensional basins. Earth Planet Sci Lett 150:7–26

Cahen L, Lepersonne J (1981) Late Palaeozoic tillites of the Congo Basin in Zaire. In: Hambrey MJ, Harland WB (eds) Earth's pre-Pleistocene glacial record. Cambridge University Press, Cambridge, pp 43–47

Cahen L, Ferrand JJ, Haarsma MJF, Lepersonne J, Verbeek T (1959) Description du Sondage de Samba: Ann Mus roy Afr cent, Tervuren (Belgique), Série in-8°, Sciences géologiques 29

Catuneanu O, Wopfner H, Eriksson PG, Cairncross B, Rubidge BS, Smith RMH, Hancox PJ (2005) The Karoo basins of south-central Africa. J Afr Earth Sci 43:211–253

Delvaux D (1991) The Karoo to Recent Rifting in the Western Branch of the East-African Rift System: a Bibliographical Synthesis. Mus roy Afr centr, Tervuren (Belg). Dept Geol Min, Rapp ann 1989–1990:63–83

Delvaux D (2001) Karoo rifting in western Tanzania: precursor of Gondwana break-up? In: Contributions to geology and paleontology of Gondwana. In honour of Prof. Dr. Helmut Wopfner, Cologne, pp 111–125

Delvaux D, Kervyn F, Macheyeki AS, Temu EB (2012) Geodynamic significance of the TRM segment in the East African Rift (W-Tanzania): active tectonics and paleostress in the Ufipa plateau and Rukwa basin. J Struct Geol 37:161–180

Donelick RA, Ketcham RA, Carlson WD (1999) Variability of apatite fission-track annealing kinetics II: crystallographic orientation effects. Am Min 84:1224–1234

Donelick RA, O'Sullivan PB, Ketcham RA (2005) Apatite fission-track analysis. Rev Mineral Geochem 58:49–94

Dunkl I (2002) Trackkey: a Windows program for calculation and graphical presentation of fission track data. Comput Geosci 28:3–12

Ebinger CJ (1989) Tectonic development of the western branch of the East African rift system. Geol Soc Am Bull 101:885–903

Ebinger CJ, Furman T (2002) Geodynamical setting of the Virunga Volcanic Province, East Africa. Acta Vulcanol 14:1–8

Ebinger CJ, van Wijk J, Keir D (2013) The time scales of continental rifting: implications for global processes. Geol Soc Am Spec Pap 500:1–13

Ehlers TA, Chaudhri T, Kumar S, Fuller CW, Willett SD, Ketcham RA, Brandon MT et al (2005) Computational tools for low-temperature thermochronometer interpretation. Rev Mineral Geochem 58:589–622

Emmel B, Jöns N, Kroener A, Jacobs J, Wartho J-A, Schenk V, Razakamanana T, Austegard A (2008) From closure of the mozambique ocean to gondwana breakup: new evidence from geochronological data of the vohibory terrane, Southwest Madagascar. J Geol 116:21–38

Eyles N (2008) Glacio-epochs and the supercontinent cycle after ~3.0 Ga: tectonic boundary conditions for glaciation. Palaeogeogr Palaeocl 258:89–129

Fabre J (1988) Les séries Paléozoiques d'Afrique: une approche. J Afr Earth Sci 7:1–40

Farley KA (2000) Helium diffusion from apatite: general behaviour as illustrated by Durango fluorapatite. J Geophys Res 105(B2):2903–2914

Farley KA (2002) (U–Th)/He dating: techniques, calibrations, and applications. Rev Mineral Geochem 47:819–844

Farley KA (2007) He diffusion systematic in minerals: evidence from synthetic monazite and zircon structure phosphates. Geochim Cosmochim Acta 71:4015–4024

Farley KA, Wolf RA, Silver LT (1996) The effects of long-alpha-stopping distances on (U–Th)/He ages. Geochim Cosmochim Acta 60:4223–4229

Fitzgerald PG, Baldwin SL, Webb LE, O'Sullivan PB (2006) Interpretation of (U–Th)/He single grain ages from slowly cooled crustal terranes: a case study from the Transantarctic Mountains of southern Victoria Land. Chem Geol 225:91–120

Flowers RM (2009) Exploiting radiation damage control on apatite (U–Th)/He dates in cratonic regions. Earth Planet Sci Lett 277:148–155

Flowers RM, Bowring SA, Reiners PW (2006) Low long-term erosion rates and extreme continental stability documented by ancient (U–Th)/He dates. Geology 34:925–928

Flowers RM, Ketcham RA, Shuster DL, Farley KA (2009) Apatite (U–Th)/He thermochronometry using a radiation damage accumulation and annealing model. Geochim Cosmochim Acta 73:2347–2365. doi:10.1016/j.gca.2009.01.015

Foster DA, Gleadow AJW (1992) The morphotectonic evolution of rift-margin mountains in central Kenya: constraints from apatite fission-track thermochronology. Earth Planet Sci Lett 113:157–171

Foster DA, Gleadow AJW (1996) Structural framework and denudation history of the flanks of the Kenya and Anza Rifts, East Africa. Tectonics 15:258–271

Fritz H, Tenczer V, Hauzenberger CA, Wallbrecher E, Hoinkes G (2005) Central Tanzanian tectonic map: a step forward to decipher Proterozoic structural events in the East African Orogen. Tectonics 24:TC6013

Galbraith RF (1981) On statistical models for fission track counts. Math Geol 13:471–478

Gleadow AJW, Duddy IR (1981) A natural longterm track annealing experiment for apatite. Nucl Tracks 5:169–174

Green PF (1981) 'Track-in track' length measurements in annealed apatites. Nuclear Tracks 5:121–128

Green PF (1988) The relationship between track shortening and fission track age reduction in apatite: combined influences of inherent instability, annealing anisotropy, length bias and system calibration. Earth Planet Sci Lett 89:335–352

Green PF, Durrani SA (1977) Annealing studies of tracks in crystals. Nucl Track Detect 1:33–39

Green PF, Duddy IR, Gleadow AJW, Tingate PR, Laslett GM (1986) Thermal annealing of fission tracks in apatite, 1. A qualitative description. Chem Geol 59:237–253

Green PF, Crowhurst PV, Duddy IR, Japsen P, Holford SP (2006) Conflicting (U–Th)/He and fission track ages in apatite: enhanced He retention, not anomalous annealing behaviour. Earth Planet Sci Lett 250:407–427

Green PF, Lidmar-Bergström K, Japsen P, Bonow JM, Chalmers JA (2013) Stratigraphic landscape analysis, thermochronology and the episodic development of elevated, passive continental margins. Geol Surv Den Greenl Bull 30:1–150

Guenthner WR, Reiners PW, Ketcham RK, Nasdala L, Giester G (2013) Helium diffusion in natural zircon: radiation damage, anisotropy, and the interpretation of zircon (U–Th)/He thermochronology. Am J Sci 313:145–198. doi:10.2475/03.2013.01

Guiraud R, Bosworth W, Thierry J, Delplanque A (2005) Phanerozoic geological evolution of Northern and Central Africa: an overview. J Afr Earth Sci 43:83–148

Hourigan JK, Reiners PW, Brandon MT (2005) U–Th zonation-dependent alpha-ejection in (U–Th)/He chronometry. Geochim Cosmochim Acta 69:3349–3365

Isbell JL, Henry LC, Gulbranson EL, Limarino CO, Fraiser ML, Koch ZJ, Ciccioli PL, Dineen AA (2012) Glacial paradoxes during the late Paleozoic ice age: evaluating the equilibrium line altitude as a control on glaciation. Gondwana Res 22:1–19

Kadima E, Delvaux D, Sebagenzi SN, Tack L, Kabeya SM (2011) Structure and geological history of the Congo Basin: an integrated interpretation of gravity, magnetic and reflection seismic data. Basin Res 23:499–527

Kampunzu AB, Bonhomme MG, Kanika M (1998) Geochronology of volcanic rocks and evolution of the Cenozoic Western Branch of the East African Rift System. J Afr Earth Sci 26:441–461

Karl M, Glasmacher UA, Kollenz S, Franco-Magalhaes AOB, Stockli DF, Hackspacher PC (2013) Evolution of the South Atlantic passive continental margin in southern Brazil derived from zircon and apatite (U–Th–Sm)/He and fission-track data. Tectonophysics 604:224–244

Karner GD, Byamungu BR, Ebinger CJ, Kampunzu AB, Mukasa RK, Nyakaana J, Rubondo ENT, Upcott NM (2000) Distribution of crustal extension and regional basin architecture of the Albertine rift system, East Africa. Mar Petrol Geol 17:1131–1150

Kaufmann G, Romanov D (2012) Landscape evolution and glaciation of the Rwenzori Mountains, Uganda: insights from numerical modeling. Geomorphology 138:263–275. doi:10.1016/j.geomorph.2011.09.011

Ketcham RA (2005) Forward and Inverse Modelling of low-temperature thermochronometry data. In: Reiners PW, Ehlers TA (eds) Low-temperature thermochronology: techniques, interpretations and applications, vol 58. Reviews in Mineralogy and Geochemistry, pp 275–314

Ketcham RA (2013) HeFTy version 1.8.0, manual

Ketcham RA, Carter A, Donelick RA, Barbarand J, Hurford AJ (2007) Improved modeling of fission-track annealing in apatite. Am Mineral 92:799–810

Ketcham RA, Donelick RA, Balestrieri ML, Zattin M (2009) Reproducibility of apatite fission-track length data and thermal history reconstruction. Earth Planet Sci Lett 284:504–515

Koehn D, Lindenfeld M, Rümpker G, Aanyu K, Haines S, Passchier C (2010) Active transsection faults in rift transfer zones: evidence for rotating stress fields in the East African Rift and implications for crustal fragmentation processes. Int J Earth Sci 99:1633–1642

Kusznir NJ, Ziegler PA (1992) The mechanics of continental extension and sedimentary basin formation: a simple-shear/pure-shear flexural cantilever model. Tectonophysics 215:117–131

Laslett GM, Gleadow AJW, Duddy IR (1984) The relationship between fission track length and track density distributions. Nucl Tracks Radiat Meas 9:29–38

Lemke P, Ren J, Alley RB, Allison I, Carrasco J, Flato G, Fujii Y, Kaser G, Mote P, Thomas RH, Zhang T (2007) Observations: changes in snow, ice and frozen ground. In: Solomon S, Qin D, Manning M, Chen Z, Marquis M, Averyt KB, Tignor M, Miller HL (eds) Climate change 2007: the physical science basis. Contribution of working group I to the fourth assessment report of the intergovernmental panel on climate change. Cambridge University Press, Cambridge and New York, NY

Lepersonne J (1974) Carte Géologique du Zaire, Èchelle 1:2,000,000—Republique du Zaire, Commissariate d'Etat aux Mines, Service Géologique

Link K, Koehn D, Barth MG, Tiberindwa JV, Barifaijo E, Aanyu K, Foley SF (2010) Continuous cratonic crust between the

Congo and Tanzania blocks in western Uganda. Int J Earth Sci 99:1559–1573. doi:10.1007/s00531-010-0548-8
Lisker F, Ventura B, Glasmacher UA (2009) Apatite thermochronology in modern geology. Geol Soc Lond Spec Publ 324:1–23
Livingstone DA (1967) Vegetation of the Ruwenzori Mountains in Equatorial Africa. Ecol Monogr 37:25–52
Macheyeki AS, Delvaux D, De Batist M, Mruma A (2008) Fault kinematics and tectonic stress in the seismically active Manyara-Dodoma Rift segment in Central Tanzania—implications for the East African Rift. J Afr Earth Sci 51:163–188
MacPhee D (2006) Exhumation, Rift-flank uplift, and Thermal Evolution of the Rwenzori Mountains Determined by Combined (U–Th)/He and U–Pb thermochronometry. Master thesis, Massachusetts Institute of Technology
Mbede EL (2001) Tectonic setting and uplift analysis of the Pangani Rift Basin in Northern Tanzania using apatite fission track thermochronology. Tanz J Sci 27A Abstr Vol Spec Issue: 23–36
McConnell RB (1959) Outline of the geology of the Ruwenzori Mountains, a preliminary account of the results of the British Ruwenzori expedition, 1951–1952. Overseas Geol Miner Resour 7:245–268
Michot F (1938) Etude pétrographique et géologique du Ruwenzori septentrional. Mém. Inst Rroy Ccolon Belg Sect Sc Nat et Med 8:66–271
Morley CK (1999) Tectonic evolution of the East African Rift System and the modifying influence of magmatism: a review. Acta Vulcanol 11:1–19
Noble WP, Foster DA, Gleadow AJW (1997) The post-Pan-African thermal and extensional history of the crystalline basement rocks in eastern Tanzania. Tectonophysics 275:331–350
Ollier CD, Pain CF (2000) The origin of mountains. Routledge, London
Osmaston HA, Harrison SP (2005) The late Quaternary glaciation of Africa: a regional synthesis. Quatern Int 138:32–54
Ovington T, Burdon P (2009) Upper Pliocene Fluvio-Deltaic Reservoirs of the Victoria Nile/Butiaba Play, Alpert Rift, Western Uganda. PESGB Conference September 2009, London
Petters SW (1991) Regional Geology of Africa. Lecture notes in Earth Sciences series, 40. Springer, Berlin, Heidelberg, New York, London, Paris, Tokyo, Hong Kong
Pickford M, Senut B, Hadoto D (1993) Geology and paleobiology of the Albertine Rift valley in Uganda-Zaire, vol I, Geology Occasional Publications, vol 24, Centre International pour la Formation et les Echanges Geologiques, Orléans
Pik R, Marty B, Carignan J, Lavé J (2003) Stability of the Upper Nile drainage network (Ethiopia) deduced from (U–Th)/He thermochronometry: implications for uplift and erosion for the Afar plume dome. Earth Planet Sci Lett 215:73–88
Pik R, Marty B, Carignan J, Yirgu G, Ayalew T (2008) Timing of East African Rift development in southern Ethiopia: implication for mantle plume activity and evolution of topography. Geology 36:167–170
Reiners PW (2005) Zircon (U–Th)/He Thermochronometry. In: Reiners PW, Ehlers TA (eds) Thermochronology, vol. 58. Reviews in Mineralogy and Geochemistry, pp. 151–176
Reiners PW, Brandon MT (2006) Using thermochronology to understand orogenic erosion. Annu Rev Earth Planet Sci 34:419–466
Reiners PW, Farley KA (2001) Influence of crystal size on apatite (U–Th)/He thermochronology: an example from the Bighorn Mountains, Wyoming. Earth Planet Sci Lett 188:413–420
Reiners PW, Nicolescu S (2006) Measurement of parent nuclides for (U–Th)/He chronometry by solution sector ICP-MS, ARHDL report 1, University of Arizona
Reiners PW, Shuster DL (2009) Thermochronology and landscape evolution. Phys Today 62:31–36
Reiners PW, Farley KA, Hickes HJ (2002) He diffusion and (U–Th)/He thermochronometry of zircon: initial results from Fish Canyon Tuff and Gold Butte. Tectonophysics 349:247–308
Reiners PW, Spell TL, Nicolescu S, Zanetti KA (2004) Zircon (U–Th)/He thermochronometry: He diffusion and comparisons with 40Ar/39Ar dating. Geochim Cosmochim Acta 68:1857–1887
Reiners PW, Ehlers TA, Zeitler PK (2005) Past, present, and future of thermochronology. In: Reiners PW, Ehlers TA (Eds) Thermochronology, vol 58. Reviews in Mineralogy and Geochemistry, pp 151–176
Ring U (2014) The East African Rift System. Austrian J Earth Sci 107:132–146
Roberts AM, Yielding G (1991) Deformation around basin-margin faults in the North Sea/mid Norway rift. In: Roberts AM, Yielding G, Freeman B (eds) The Geometry of Normal Faults, vol 56. Special Publications of the Geological Society of London, London, pp 61–78
Roberts EM, Stevens NJ, O'Connor PM, Dirks PHGM, Gottfried MD, Clyde WC, Armstrong RA, Kemp AIS, Hemming S (2012) Initiation of the western branch of the East African Rift coeval with the eastern branch. Nat Geosci 5:289–294
Roller S, Hornung J, Hinderer M, Ssemmanda I (2010) Middle Miocene to Pleistocene sedimentary record of rift evolution in the southern Albertine Rift (Uganda). Int J Earth Sci 99:1643–1661. doi:10.1007/s00531-010-0560-z
Roller S, Wittmann H, Kastowski M, Hinderer M (2012) Erosion of the Rwenzori Mountains, East African Rift, from in situ-produced cosmogenic 10 Be. J Geophys Res 117:F03003
Rowley DB, Sahagian D (1986) Depth-dependent stretching: a different approach. Geology 14:32–35
Royden L, Keen CE (1980) Rifting process and thermal evolution of the continental margin of eastern Canada determined from subsidence curves. Earth Planet Sci Lett 51:343–361
Sachau T, Koehn D (2010) Faulting the lithosphere during extension and related rift-flank uplift, a numerical study. Int J Earth Sci 99:1619–1632. doi:10.1007/s00531-010-0513-6
Schlueter T (1997) Geology of East Africa. Gebr Bortntraeger, Berlin, Stuttgart
Schlueter T, Picho-Olarker G, Kreuser T (1993) A review of some neglected Karoo grabens of Uganda. J Afr Earth Sci 17:415–428
Shuster DL, Farley KA (2009) The influence of artificial radiation damage and thermal annealing on helium diffusion kinetics in apatite. Geochim Cosmochim Acta 73:183–196
Shuster DL, Flowers RM, Farley KA (2006) The influence of natural radiation damage on helium diffusion kinetics in apatite. Earth Planet Sci Lett 249:148–161
Spiegel C, Kohn BP, Belton DX, Gleadow AJW (2004) Integrating apatite fission track and (U–Th)/He data: the thermal evolution of rift-valley flanks in central Kenya. Abstract book, International fission-track conference 2004, Amsterdam
Spiegel C, Kohn BP, Belton DX, Gleadow AJW (2007) Morphotectonic evolution of the central Kenya rift flanks: implications for late Cenozoic environmental change in East Africa. Geology 35:427–430
Spiegel C, Kohn BP, Belton DX, Berner Z, Gleadow AJW (2009) Apatite (U–Th–Sm)/He thermochronology of rapidly cooled samples: the effect of He implantation. Earth Planet Sci Lett 285:105–114
Tack L, Wingate MTD, De Waele B, Meert J, Belousova E, Griffin B, Tahon A, Fernandez-Alonso M (2010) The 1375 Ma "Kibaran event" in Central Africa: prominent emplacement of bimodal magmatism under extensional regime. Precambrian Res 180:63–84
Tanner PWG (1971) The Stanley Volcanics formation of Ruwenzori, Uganda. Fifteenth annual report of the Research Institute of African Geology, University of Leeds

Thomson SN, Brandon MT, Tomkin JH, Reiners PW, Vásquez C, Wilson NJ (2010) Glaciation as a destructive and constructive control on mountain building. Nature 147:313–317
Tugume FA, Nyblade AA (2009) The depth distribution of seismicity at the northern end of the Rwenzori Mountains; implications for heat flow in the western branch of the East African Rift system in Uganda. S Afr J Geol 112:261–276
Upcott NM, Mukasa RK, Ebinger CJ (1996) Along-axis segmentation and isostasy in the Western rift. East Afr J Geophys Res 101(B2):3247–3268
Ring U (2008) Extreme uplift of the Rwenzori Mountains in the East African Rift, Uganda: structural framework and possible role of glaciations. Tectonics 27:TC4018. doi:10.1029/2007TC002176
van der Beek P, Cloetingh S, Andriessen P (1994) Mechanisms of extensional basin formation and vertical motions at rift flanks: constraints from tectonic modelling and fission-track thermochronology. Earth Planet Sci Lett 121:417–433
van der Beek P, Mbede E, Andriessen P, Delvaux D (1998) Denudation history of the Malawi and Rukawa Rift flanks (East African Rift System) from apatite fission track thermochronology. J Afr Earth Sci 26:363–385
Vermeesch P (2009) Radial Plotter: a Java application for fission track, luminescence and other radial plots. Radiat Meas 44:409–410
Vermeesch P, Seward D, Latkoczy C, Wipf M, Guenther D, Baur H (2007) Alpha-emitting mineral inclusions in apatite, their effect on (U–Th)/He ages, and how to reduce it. Geochim Cosmochim Acta 71:1737–1746
Wagner GA (1972) Spaltspurenalter von Mineralen und natürlichen Gläsern: eine Übersicht. Fortschr Miner 49:114–145
Wagner GA, Van den haute P (1992) Fission-track dating. Enke, Stuttgart
Wagner M, Altherr R, Van den haute P (1992) Apatite fission-track analysis of Kenyan basement rocks: constraints on the thermotectonic evolution of the Kenya dome. A reconnaissance study. Tectonophysics 204:93–110
Whittow JB (1966) The landforms of the Central Ruwenzori. East Afr Geogr J 132:32–42
Wolf RA, Farley KA, Kass DM (1998) Modeling of the temperature sensitivity of the apatite (U–Th/He) thermochronometer. Chem Geol 148:105–114